

Journal Pre-proof

Synergistic Effects of Optimizing Stir Casting and Friction Stir Welding for WC and Al₂O₃ based Nano-Particulates Reinforced AA2014 and AA6061 Alloys: Mechanical, Weldability, Corrosion, and Microstructural Morphological Insights

Balram Yelamasetti, Chilakamarri L. Aslesha, Vijaya Sarathi T, Rajyalakshmi G, Sagar Shelare, Shubham Sharma, Jasmina Lozanovic, A.I. Ismail

PII: S2238-7854(25)00387-4

DOI: <https://doi.org/10.1016/j.jmrt.2025.02.140>

Reference: JMRTEC 13092

To appear in: *Journal of Materials Research and Technology*

Received Date: 11 December 2024

Revised Date: 13 February 2025

Accepted Date: 14 February 2025

Please cite this article as: Yelamasetti B, Aslesha CL, Sarathi T V, G R, Shelare S, Sharma S, Lozanovic J, Ismail A, Synergistic Effects of Optimizing Stir Casting and Friction Stir Welding for WC and Al₂O₃ based Nano-Particulates Reinforced AA2014 and AA6061 Alloys: Mechanical, Weldability, Corrosion, and Microstructural Morphological Insights, *Journal of Materials Research and Technology*, <https://doi.org/10.1016/j.jmrt.2025.02.140>.

This is a PDF file of an article that has undergone enhancements after acceptance, such as the addition of a cover page and metadata, and formatting for readability, but it is not yet the definitive version of record. This version will undergo additional copyediting, typesetting and review before it is published in its final form, but we are providing this version to give early visibility of the article. Please note that, during the production process, errors may be discovered which could affect the content, and all legal disclaimers that apply to the journal pertain.

© 2025 Published by Elsevier B.V.



Synergistic Effects of Optimizing Stir Casting and Friction Stir Welding for WC and Al₂O₃ based Nano-Particulates Reinforced AA2014 and AA6061 Alloys: Mechanical, Weldability, Corrosion, and Microstructural Morphological Insights

Balram Yelamasetti^{1*}, Chilakamarri L Aslesha², Vijaya Sarathi T³, Rajyalakshmi G⁴, Sagar Shelare^{5,6}, Shubham Sharma^{7,8,9,10*}, Jasmina Lozanovic^{11*}, AI Ismail¹²

¹Department of Mechanical Engineering, MLR Institute of Technology, Hyderabad, Telangana-500043, India. Balram3072@gmail.com (BY)

²Department of Mechanical Engineering, Vignan's Institute of Engineering for Women, Visakhapatnam-530049, Andhra Pradesh, India. chilakamarriaslesha@gmail.com (CLA)

³Department of Mechanical Engineering, B.V. Raju Institute of Technology, Narsapur, Telangana-502313, India. vijayasarathi.t@bvrit.ac.in (VST)

⁴Department of Manufacturing Engineering, Vellore Institute of Technology, Vellore, Tamil Nadu, 632 014, India. rajyalakshmi@vit.ac.in (RG)

⁵Department of Mechanical Engineering, Priyadarshini College of Engineering, Nagpur, 440019, Maharashtra, India. sagmech24@gmail.com (SS)

⁶Chitkara Centre for Research and Development, Chitkara University, Himachal Pradesh, 174103, India.

⁷Department of Technical Sciences, Western Caspian University, Baku, Azerbaijan. shubham543sharma@gmail.com, shubhamsharmacsirclri@gmail.com (S.S.)

⁸Centre for Research Impact and Outcome, Chitkara University Institute of Engineering and Technology, Chitkara University, Rajpura-140401, Punjab, India. E-Mail: shubham543sharma@gmail.com, shubhamsharmacsirclri@gmail.com (S.S.)

⁹School of Mechanical and Automotive Engineering, Qingdao University of Technology, Qingdao, 266520, China. shubham543sharma@gmail.com, shubhamsharmacsirclri@gmail.com (SS)

¹⁰Jadara University Research Center, Jadara University, Jordan. E-Mail: shubham543sharma@gmail.com, shubhamsharmacsirclri@gmail.com (S.S.)

¹¹University of Applied Sciences Campus Vienna, Department of Engineering, 1100, Vienna, Austria. jasmina.lozanovic@fh-campuswien.ac.at (JL)

¹²Mechanical engineering Department, College of engineering and architecture, UMM Alqura University, Saudi Arabia. aiismail@uqu.edu.sa

***Corresponding author emails:** shubham543sharma@gmail.com, shubhamsharmacsirclri@gmail.com (SS); jasmina.lozanovic@fh-campuswien.ac.at (JL); balram3072@gmail.com (BY); sagmech24@gmail.com (SS)

Abstract: This paper aims to investigate metallurgical changes and mechanical properties of stir casted AA2014 and AA6061 metal matrix composites and their as-weld condition developed with FSW technique. The composites, AA2014 and AA6061 were developed by adding 5% WC and 5% Al₂O₃ using stir casting process to study the impact of nano-particulates on material's properties. The stir casting developed samples were joined using FSW process using square tool to investigate the weldability, weld strength quality, wear and corrosion behavior. In addition, the microstructural changes due to the nano-particulates and welding process at the weld zone were reported. The tensile strength and micro-hardness were evaluated by applying uni-axial loads and indentation loads on the surface, respectively. Wear rate and corrosion resistance of FSW dissimilar joint were measured by using pin-on-disc and cyclic sweep tests, respectively. The UTS of AA2014 and AA6061 stir casted composites was observed as 155 and 184 MPa respectively whereas the UTS of dissimilar welded AA2014 and AA6061 composites was observed as 156 MPa with std. deviation of ± 2 . The average micro-hardness number is observed as 116 HV for AA2014 and 46 HV for AA6061 stir casted samples. The hardness number was increased in HAZ and TMAZ of AA2014 side in FSW joint as compared to stir casted composite. The FSW welded sample showed excellent resistance to environmental degradation with a low corrosion rate of 0.0131563 mm/year and excellent wear resistance, as evidenced by a less wear depth of 20 microns. Microstructures revealed that the nugget zone is exhibited with uniform, defect-free joints with evenly distributed reinforcement phases. The findings highlight the material's suitability for lightweight, durable components in aerospace, automotive, and marine industries.

Keywords: Stir casting; AA2014 and AA6061 Alloys; Friction stir welding; Mechanical characterization; metallurgical studies, wear and corrosion rate.

Nomenclature:

Friction Stir Welding – FSW

Tungsten Inert Gas –TIG

Tungsten Carbide – WC

Aluminium Alloys Metal Matrix Composites – AAMMC

Electrical Discharge Machining – EDM

American Society for Testing and Materials – ASTM

Optical Microscope – OM

Scanning Electron Microscopy – SEM

Energy Dispersive X-ray Spectroscopy – EDS

Co-efficient of Friction – COF

Ultimate Tensile Strength – UTS

Yield Strength – YS

Base Metal – BM

Heat-Affected Zone – HAZ

Thermo-Mechanically Affected Zone – TMAZ

1. Introduction

AA2014 is a copper-based alloy that possesses exceptional strength and outstanding machining properties. AA2014 is frequently employed in numerous aerospace structural applications owing to its exceptional strength [1]. AA6061 mostly consists of magnesium and silicon which is usually precipitation hardened. It possesses favorable mechanical properties, demonstrates excellent weldability, and is widely used alloy of Al for general-purpose applications [2]. Due to excellent properties, such as being lightweight, having a very high strength-to-weight ratio, and corrosion resistance, Al forms the basis for advanced composites. Incorporation of reinforcements in Al leads to MMCs that realize high mechanical and thermal property enhancements, making it very appropriate for modern engineering applications.

Researchers have fabricated the MMCs by reinforcing nano-particulates to produce the desired mechanical properties. To list a few, Kumar et al. [3] studied the mechanical and tribological properties of Al matrix composites reinforced by WC through stir casting technique. This study concludes that the hardness along with tensile strength and wear resistance due to the addition of WC is improved, while increased ductility is observed by increasing the content of WC. Deep et al. [4] used ultrasonic-assisted stir-squeeze casting to investigate the impact of Al₂O₃ nanoparticles in AA5456 alloy hybrid nanocomposites. It was observed that Al₂O₃ nanoparticles enhanced the density, hardness (158.64 HV), and mechanical properties of the composite significantly. The yield strength increased by 51.02% and the ultimate tensile strength by 35.32%. Grain boundary strengthening and an increase in overall compressive strength were also influenced by the addition of Al₂O₃ nanoparticles. Long et al. [5] considered the reinforcing influence of nano-WC in an AlSi10Mg alloy using an in-situ surface modification method. The UTS value with addition of 3wt.% of nano-WC is increased to 464 MPa and a corresponding elongation of 5.6%. The addition of nano-WC particles contributed towards a columnar-to-equiaxed microstructure transition that had a significant contribution in increasing the strength and wear resistance.

The welding of Al alloys is challenging due to its susceptibility to produce welding defects [6]. FSW is a solid state joining technique used especially for joining Al alloys, with weld strength that is superior to the base metal and minimal distortion, which are critical for maintaining the lightweight and high-performance characteristics. FSW utilizes a revolving tool made of a durable material with a specified shape to generate heat through friction and soften it to join two different materials [7, 8]. The benefits of FSW encompass enhanced efficiency, reduced energy consumption, increased tensile and fatigue strength, the ability to weld thicker sections without flash, absence of filler material, and simpler edge preparation [9,

10]. In addition, it mitigates welding defects such as solidification cracking, deformation, and porosity that are prevalent in the fusion welding process [9, 10].

To attain the highest quality weld, it is crucial to comprehend the impact of process factors, particularly the axial force, welding speed and rotating speed. Xavier et al. [11] adapted FSW to create lap and butt joints of AA2014-T6 alloys at varying process parameters such as pin length, shoulder diameter, major and minor diameters of pin, rotation speed and transverse speed and emphasized the importance of selecting the right tool and process parameters for a high-quality weld, highlighting the significance of plastic deformation, material flow, and recrystallization. Kannaiyan et al. [12] studied the defects of FSW AA5083 and AA6061-T6 weldments using acoustic emission techniques. They found that defect-free welds had the highest tensile strength and superior hardness, while pinhole and pipe defects showed significant variances due to their larger defect regions. The cracked areas showed fractures that occurred in a ductile nature, characterized by elongated dimples and micro-voids. The study by Bindhushree et al. [13] examined FSW of cast A356 and A2014 alloys, analyzing the effects of various parameters like tool pin shape, rotation speed, and welding speed. The results showed complete joining of parent alloys, no micro-porosities, and re-crystallization forming smaller grains. Rana et al. [14] studied on welded butt- welded joints of AA7075 and AA6061 and revealed that the combination of TIG welding and FSW resulted in higher mechanical strength and hardness in the nugget zone. The refined grain structures and defect-free bonding were obtained through the combined use of TIG and FSW techniques.

The tool rotational speed significantly impacts FSW, influencing heat formation, material flow, and microstructure evolution. Kar et al. [15] investigated the mechanical characteristics of FSW of Al alloys to titanium alloy and observed that increased speeds improve material plasticity and weld mixture mixing, while excessive speeds can cause overheating and defects. In another study, Zhu et al. [16] observed that excessively high rotational speeds can cause overheating, which in turn can lead to the formation of coarse grains and the occurrence of defects such as voids and tunnel formation. The traverse speed impacts the thermal cycle and the rate at which the material cools down, Wang et al. [17]. The investigation on under water FSW of Al-Mg-Si, Sabry et al. [18], observed that the increased traverse speed resulted in decreased heat input, which in turn leads to the formation of smaller grain structures and enhanced mechanical characteristics. On the contrary, Essa et al. [19] inferred that, reducing the pace at which the weld is made might lead to a higher amount of heat being applied, particularly in AA5083 and AA7075 alloys, causing the material to become softer and resulting in a decrease in the quality of the weld. In FSW of AA2024-T6, Tobin et al. [20] investigated that the axial force has an impact on both the depth of penetration as well as the material strength. In another study on FSW, Caetano et al. [21] concluded that the effective control over the axial force enables adequate mixing of materials and the formation of bonds, while avoiding excessive tool erosion. Li et al. [22] investigated the effect of welding

time on the properties of ultrasonic spot-welded AA7075-T6 and casting Al alloy A380. The findings indicated that the increase in welding time increased the peak temperature and enhanced the shear tensile strength when compared to base metals. Sun et al. [23] discussed the influence of ZrB₂ and Al₂O₃ nanoparticles on friction stir welded 7085Al matrix composites regarding their microstructure and mechanical characteristics. The weld nugget grains are refined to 1.82 μm , whereas MgZn₂ re-precipitation is enhanced via accelerated heterogeneous nucleation due to Al₂O₃, which caused dynamic recrystallization. The improvement in ultimate tensile strength has been achieved by adding 3 vol.% of Al₂O₃ to reach a value of 492.95 MPa and elongation to 12.87% with a joint efficiency of 76.3%.

The above studies demonstrate significant improvements in mechanical properties of Al alloys, through the incorporation of nanoparticles like WC and Al₂O₃ and processing techniques via stir casting and FSW. The incorporation of WC enhances hardness, wear resistance, and tensile strength, whereas Al₂O₃ enhances grain refinement and strength. FSW and stir casting facilitate the incorporation of these nanoparticles in a manner that results in stronger, wear-resistant composites. In this research, the base metals AA2014 and AA6061 are reinforced with 5% of WC and Al₂O₃ using stir casting technique to develop the composites. These stir casted composites are joined using FSW technique using a square tool pin. A comprehensive assessment is carried out on both stir casted composites and FSW welded samples for mechanical properties, metallurgical changes, wear rate and corrosion resistance. The effect of reinforced particulates on Al alloys and welding characteristics are reported.

2. Material and methods

2.1 Materials

The alloys chosen in this study are AA2014 and AA6061 and the chemical composition of the metals is highlighted in Table 1. It is very important using stir casting followed by FSW because it assists in the good distribution of reinforcing particles, which are 5% WC and 5% Al₂O₃, that improve the strength and wear resistance of the composite [24]. FSW technique is used to join reinforced AAMMCs in the solid state process by employing a square tool pin geometry [25]. The methodology of the present research work is mentioned as flow chart and shown in Fig. 1.

Table 1. The chemical composition of AA2014 and AA6061 [11, 21]

Base metal	Cu	Cr	Fe	Si	Ti	Mg	Zn	Mn	Al
AA2014	4.2	0.003	0.115	0.851	0.02	0.714	0.032	-	Balance
AA6061	0.15	0.05	0.5	0.5	-	0.8	0.03	0.1	Balance

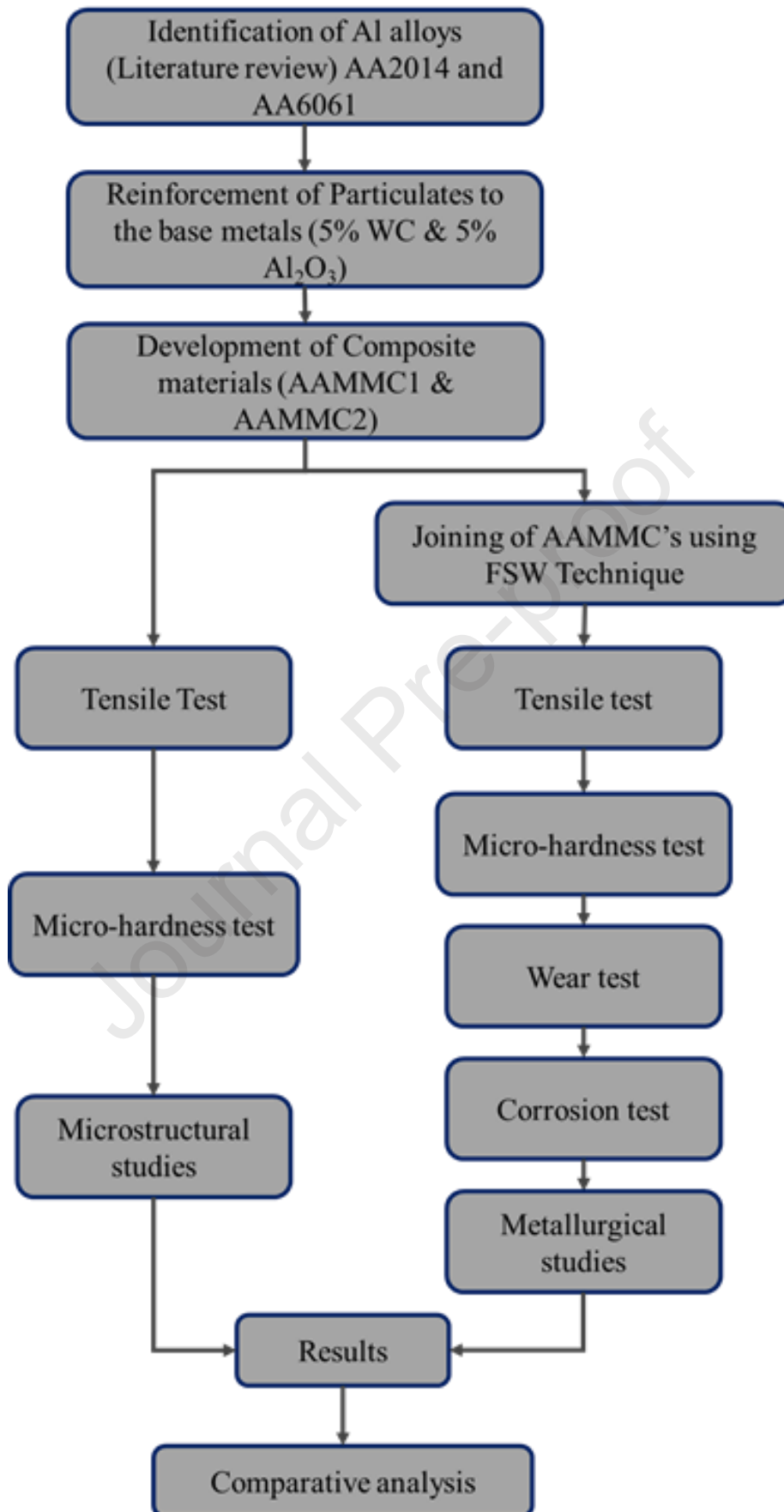


Fig. 1 The methodology followed in the present study

2.2 Stir casting of AA2014 and AA6061 to produce AAMMC

The stir casting process is a widely used technique for making metal matrix composites, ensuring that the reinforcing particles are evenly spread throughout the metal matrix. The process involves heating the matrix metal, which consists of AA6061 and AA2014 Al alloys, until they melt at the necessary temperature. The Fig. 2(a) portrays the crucible employed for the fusion of the Al alloys. After the metal has completely melted, the reinforcement particulates, consisting of 5% WC and 5% Al₂O₃, are introduced into the molten metal to prepare AAMMC samples with combinations of AA2014+5%WC+5%Al₂O₃ (AAMMC1) and AA6061+5%WC+5%Al₂O₃ (AAMMC2). The Fig. 2(b) depicts the arrangement for supplying heat to the crucible; the liquefied blend is aggressively agitated to ensure the uniform dispersion of the reinforcing particles within the substance, as illustrated in Fig. 2(c) of the stirring mechanism. Figure 2(d) presents the process of pouring the molten mixture into molds. Once the molten composite has been thoroughly mixed, it is poured into molds that have been prepared in advance. The composite then solidifies in these molds, taking on the desired shape, where the cast specimens are marked and readied for further testing.



Fig. 2. Stir casting of AA2014, AA6061 with 5%WC and 5%Al₂O₃

2.3 Friction stir welding of AAMMCs

Two AAMMCs stir casted plates, of 150 × 60 × 6 mm each, were utilized in the FSW. The AAMMCs plates were thoroughly prepared by cleansing their surfaces to eliminate any

impurities and thereafter firmly fastened to prevent any displacement during the welding procedure. The process parameters were chosen examining the literature and by considering the capabilities of the FSW machine utilized, Kumar et al. [26]. The FSW machine has a capacity of 12 kVA/440V and offers a speed range of 300 to 3000 rpm. The tool material used is H13 tool steel. Profile is square pin with shoulder diameter 25 mm, pin height 5.6 mm, and tapered pin length from 7 mm at top and 5 mm at bottom. The square pin profile provides a notable advantage by generating greater frictional heat compared to alternative pin profiles. This enhances the process of softening and mixing the material. The square pin's corners produce increased shear forces, resulting in more pronounced plastic deformation, Gadakh et al. [27]. A sharper corner in a square tool will increase localized pressure, thus raising frictional heat and plastic deformation [26]. This could decrease load-bearing capacity if too much heat results in grain coarsening or defects but might increase strength if controlled dynamic recrystallization takes place [26]. Oxide layer formation might improve wear resistance but may decrease if stress concentration leads to abrasion and fatigue wear [26]. Additionally, this operation successfully disintegrates and redistributes the microstructure of the material, leading to a more consistent microstructure and improved mechanical properties of the weldments. In addition, the square pin profile equally disperses the forces throughout the whole length of the pin. This not only enhances the weld quality, but also decreases tool wear, resulting in increased durability. The developed AAMMCs FSW specimen is shown in Fig. 3.

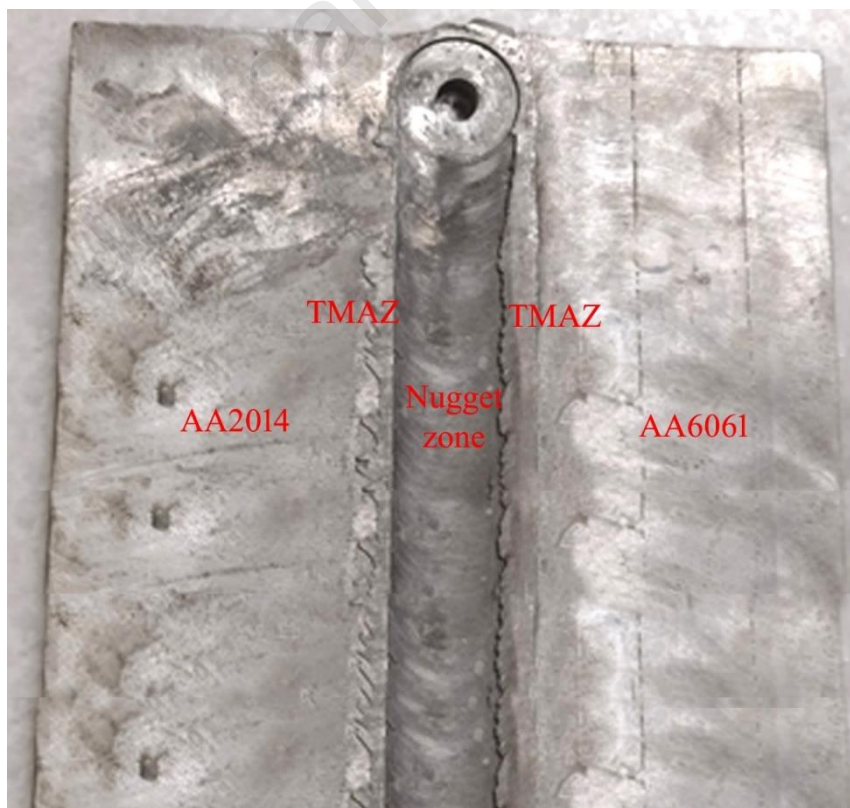


Fig. 3. Developed friction stir welded sample

2.4 Characterisation

The stir casted composites and welded samples were sliced using wire-EDM machine to conduct the various mechanical testing's and to study the microstructural changes. The tensile test (ADITYA UTE 40) was conducted by applying uni-axial loads with a shear rate of 1 mm/min as per ASTM E8 standard [12]. To determine the micro-hardness, the polished specimens were subjected to a force of 500 gf for a duration of 10 s. The micro-hardness was evaluated, by creating several indentations along the thickness of the specimen, starting from the bottom and moving towards the top, using the Vickers's Hardness tester (MATSUZAWAMMX7). Optical microscopy was utilized to examine the micro- and macro-structural properties of AAMMCs and FSW welded samples. The conventional metallurgical technique was utilized to polish the cut specimens and examine their microstructure. Keller's reagent was then applied to the polished surface. Also, SEM/EDS analysis was carried out on welded AAMMCs samples to reveal the alloy composition at various zones. The wear test was conducted to assess the tribological characteristics of the welded AAMMCs. The pin-on-disc arrangement employed to assess the wear properties in accordance with the ASTM standard G9906 [8]. The pin-on-disc arrangement comprises of an SS304 wear test specimen with a semi-circular surface that is rubbed on a hardened EN 31 steel disc. The wear test specimen was subjected to a weight of 10 N and rotated at a speed of 400 rpm while being slid for 2000 m. In addition, during the wear test, a track diameter of 80 mm was consistently maintained. The wear test had a fixed sliding duration of 20 minutes. The weight loss and COF were recorded in response to the varying sliding distances. Tafel analysis was performed following the ASTM G102 standard [11] in a 3.5 wt.% NaCl solution at a scan rate of 10 mV/s for the measurement of corrosion rate. The sample dimension was 1.5 cm² as a working electrode, and data during the scan at a particular scan rate was noted.

3. Results and discussion

3.1 Tensile test of stir casted AAMMCs

The results of the tensile test for the stir casted AAMMCs are presented in Table 2. It is observed from Table 2 that AAMMC1 has an average tensile strength of 155 MPa. The highest average tensile strength for AAMMC2 is 184 MPa and yield strength of AAMMC2 is 155 MPa. The adhesion between reinforcing particles and Al matrix is crucial for efficient load transfer, as voided interfaces can decrease tensile strength and composite material failure [28]. AAMMC1 exhibits higher ductility and elongation percentages (19.8%) than the base AA2014 alloy (13.33%) [29], indicating small reinforcement particles hinders the movement of dislocations and delays the beginning of fracture. Similar findings were observed by Gaurav et al. [30]. AAMMC2 shows a significant decrease (1.6%) in elongation and area drop (37.16%), suggesting significant necking prior to failure, but AAMMC2 saw only a minor reduction in area (0.15%), indicating a weakening impact due to reinforcing particles. Reinforcing particle dimensions, configuration, and proportion influence mechanical characteristics, with larger,

irregular particles causing stress concentrations and high proportions causing brittle behavior, reducing tensile strength [31].

The inclusion of 5% WC and 5% Al₂O₃ into AA2014 and AA6061 results in a notable changes of their mechanical properties. However, the effect on ductility varies: AAMMC1 shows decreased strength but increased ductility relative to its basic alloy. On the other hand, AAMMC2 exhibits a significant decrease in both the tensile strength and ductility, illustrating a compromise between improving hardness and wear resistance while sacrificing tensile characteristics. The observed variation in behavior suggests that the composition of the matrix alloy is a critical factor in defining the ultimate characteristics of the reinforced material.

The stress-strain curves depicted in Fig. 4 demonstrate the behavior of the casted specimens of AAMMC1 and AAMMC2 under tensile loading, showcasing their unique mechanical characteristics. The stress-strain curve for AAMMC1 demonstrates a continuous and elongated plastic deformation area, which signifies its ductility. The high strain value emphasizes the composite's capacity to experience substantial plastic deformation prior to failure, indicating that the inclusion of Al₂O₃ and WC particles does not greatly hinder its ductility [32]. Conversely, the stress-strain curve for AAMMC2 has a significantly steeper incline in the elastic zone, which is then followed by a sudden shift to failure. The highest tensile stress for AAMMC2 is around 184 MPa, surpassing that of AAMMC1, suggesting superior strength. Nevertheless, the strain at fracture for AAMMC2 exhibits a notable decrease, approximately 8%.

Table 2. The results of tensile test for AAMMCs after FSW

Sample ID	Specimens	UTS (MPa)	YS (MPa)	% of elongation	% in Reduction area
AAMMC1	1	154	68	19.8	36
	2	158	72	19.9	37.16
	3	152	67	19.6	38.32
Average		155	69	19.8	37.16
AAMMC2	1	182	154	1.8	0.15
	2	185	152	1.4	0.12
	3	186	158	1.5	0.17
Average		184	155	1.6	0.15

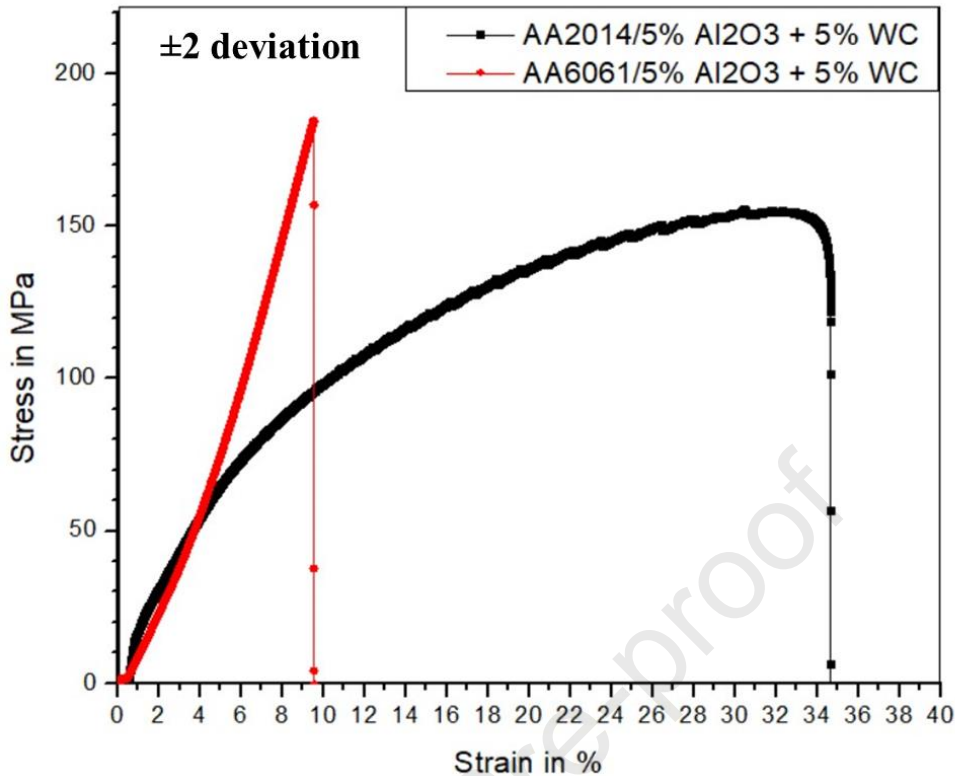


Fig. 4. The stress-strain plot for AAMMC1 and AAMMC2 after stir casting

3.2 Microstructure Analysis of stir casted AAMMCs

The microstructural examination of AAMMC1, both prior to and following etching, Fig. 5, illustrates the successful distribution of Al₂O₃ and WC particles throughout the AA2014 matrix. Uniformly distributing reinforcement particles is essential for attaining the intended mechanical properties, as it eliminates the creation of vulnerable areas and ensures continuous load transfer across the material [32]. The etching process reveals a distinct and improved grain structure, suggesting that the reinforcing particles have a substantial impact on refining the grains [33]. Performing the microstructural investigation of AAMMC2 by stir casting, as shown in Fig. 6, the Al₂O₃ and WC particles were found to be dispersed regularly throughout the AA6061 matrix. After etching, a unique pattern of dendritic grains becomes noticeable which indicates that the cooling process was fast enough to allow quick solidification [34]. The absence of significant particle clustering suggests that the stir casting method succeeded in creating a consistent composite material. Nevertheless, the existence of these particles along the interfaces between grains could also impact the composite's ability to deform, perhaps rendering it more prone to fracturing under specific loading circumstances.

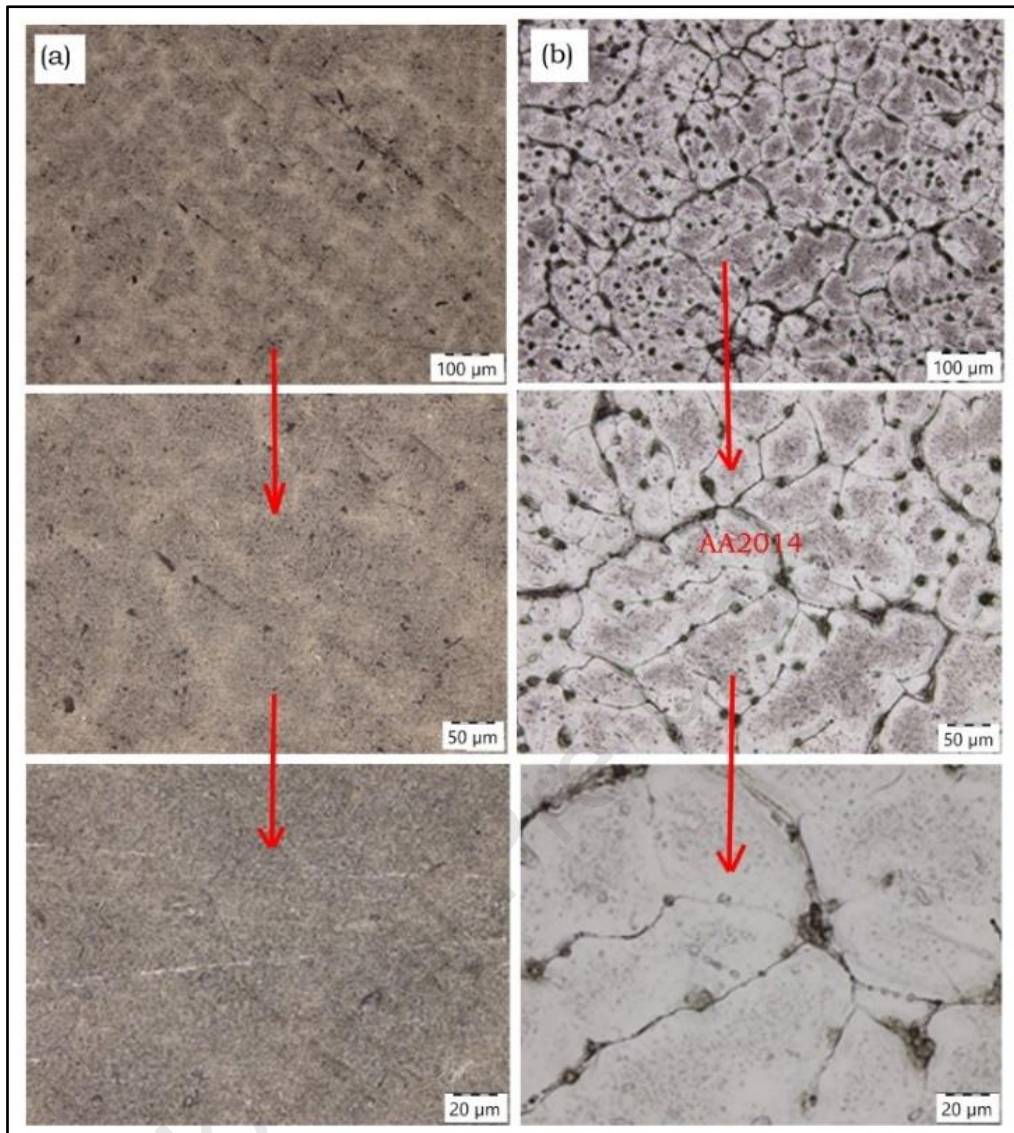


Fig. 5. The microstructures of AAMMC1 after stir casting (a) without etching at (b) with etching at different magnifications

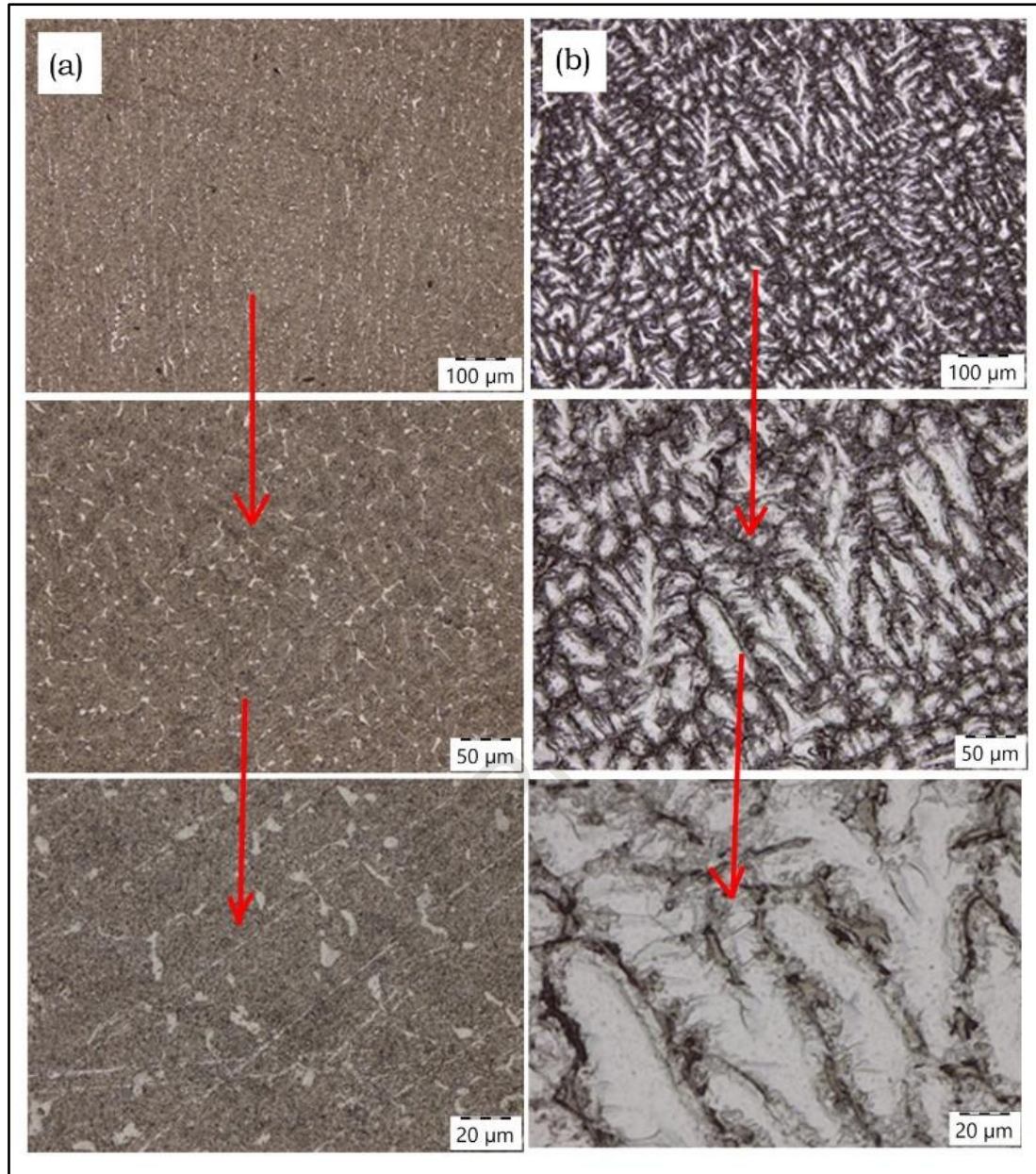


Fig. 6. The microstructures of AAMMC2 after stir casting (a) without etching at (b) with etching at different magnifications

3.3 Micro-hardness of stir casted AAMMCs

The micro-hardness test was performed on AAMMCs to study the effect reinforced nanoparticles of WC and Al_2O_3 . The AAMMC1 had an average micro-hardness number of 116 HV, which represents a significant rise in comparison to the micro-hardness of the base AA2014 alloy [29]. The notable enhancement in hardness can be ascribed to the existence of rigid ceramic particles (Al_2O_3 and WC) that are evenly dispersed inside the Al matrix. The presence of these particles hinders the migration of dislocations, which in turn improves the composite's ability to withstand plastic deformation and increases its overall hardness. In the AAMMC2, the average micro-hardness value measured 46 HV shows a significant

improvement compared to the base AA6061 alloy [29], which has an average hardness of 30 HV. The hardness enhancement is attributed to the presence of rigid ceramic particles within the matrix, enhancing the material's resistance to indentation. Despite both composites having the same type and quantity of reinforcement, AAMMC2 exhibits a decreased hardness compared to AAMMC1. The disparity may arise from the inherent characteristics of the AA6061 matrix, which could potentially have distinct interactions with the reinforcement particles in contrast to the AA2014 matrix. Moreover, the dispersion and adhesion of the particles inside the AA6061 matrix may not be as efficient as in the AA2014 matrix, leading to comparatively reduced hardness.

Table 3. The micro-hardness values for the stir casted AAMMCs

Sample Id	1 st Value	2 nd Value	3 rd Value	4 th Value	5 th Value	Avg. Value
AAMMC1	108.8	117	113	122.2	119.9	116
AAMMC2	47.7	46.9	48.9	43	44.8	46

3.4 Tensile test results of FSW AAMMCs

The tensile test result of FSW welded samples is presented in Table 4. The FSW joint between AAMMC1 and AAMMC2 has an average tensile stress of 156 MPa with yield point stress of 63 MPa. The FSW joint shows a decrease in ductility (5.96%) compared to composites, while AA2014 and AA6061 show 13.33% and 16% elongations, respectively, likely due to rigid ceramic particles. The decreased elongation indicates that the composite joint has a lower ability to undergo plastic deformation prior to fracturing. The FSW joint had a 24.28% reduction in area, indicating the extent of necking and plastic deformation the material endured before to fracture. The variations in stress-strain for the AAMMCs of weldments of FSW is illustrated in Fig. 7. The curve shows a linear relation until approximately 2% strain, which represents the material's elastic behavior. In this region, the stress increases in proportion to the strain. After this, the material undergoes plastic deformation, resulting in irreversible alterations and a deviation from the linear curve up to around 14% strain, demonstrates the material's ability to undergo plastic deformation. The presence of reinforcement particles contributes to increased strength while decreasing ductility, Raturi et al. [35].

Table 4. The tensile test results of AAMMCs after FSW

Sample ID	UTS (MPa)	YS (MPa)	% Elongation	% Reduction in area
AAMMC1 +	158	62	5.98	22.00
AAMMC2	154	64	6.97	24.22
	156	62	4.89	26.64
Average	156	63	5.96	24.28

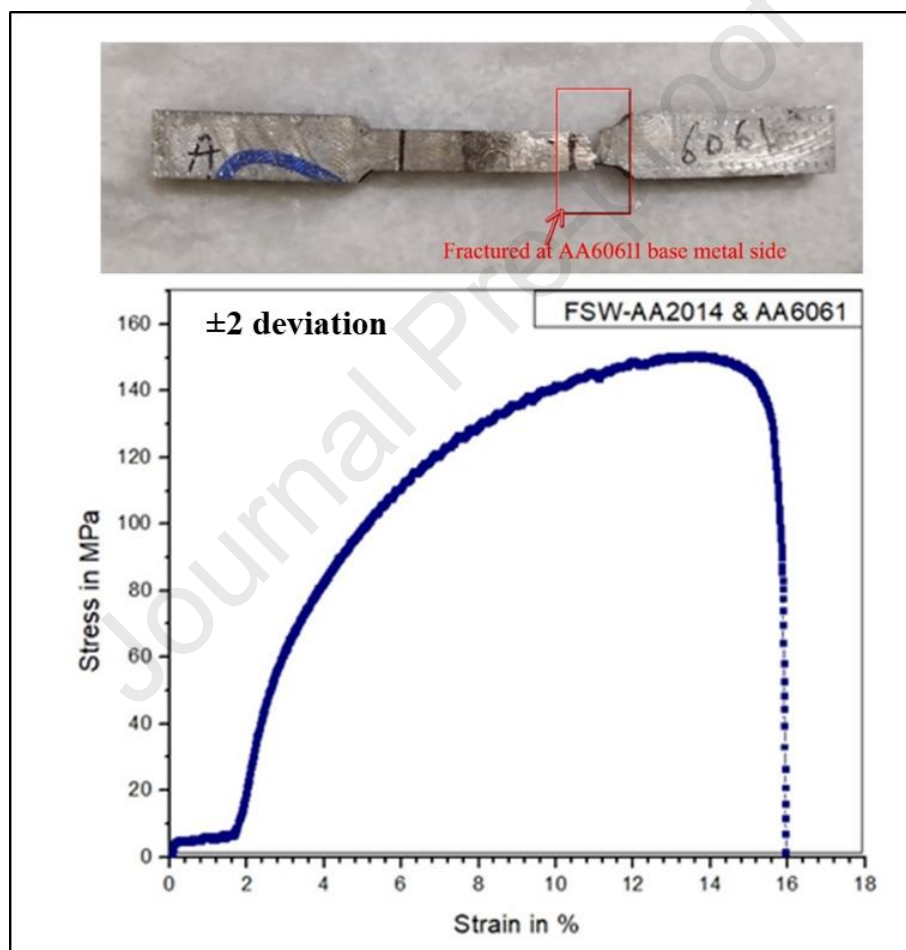


Fig. 7. The stress-strain curve for the friction stir welded AAMMCs

3.6 Micro-hardness of friction stir welded AAMMCs

The micro-hardness details of the friction stir welded AAMMCs is presented in Fig. 8. In the AA2014 base metal, the micro-hardness values exhibit a uniform pattern, with an average value of approximately 100 HV. Prior to the FSW, the AA2014 alloy exhibits consistent and even hardness. The addition of 5% Al₂O₃ and 5% WC enhanced the hardness of AA2014, making it harder. In AA6061 base metal, the micro-hardness values are relatively lower, with an average

range of approximately 40-50 HV. It is anticipated that AA6061 will be softer than AA2014, and the use of Al_2O_3 and WC reinforcements enhances the hardness, although to a smaller extent than in AA2014. The reduced hardness in AA6061 is a result of the inherent properties of the base metal, which experience a decreased strengthening effect from the additional particles, Mohan et al. [36]. The HAZ of AA2014 and AA6061 exhibit a marginal reduction in hardness when compared to the surrounding base metal areas. Abdollahzadeh et al. [37] have also observed that the decrease in strength can be attributed to the thermal cycles that occur during the FSW process may have caused the material to soften because of the dissolution or enlargement of strengthening precipitates in certain areas.

The TMAZ showed a more pronounced variation in hardness levels. On the AA2014 side, the hardness exhibits a gradual increase towards the weld zone, reaching its highest point. The increase in hardness may be attributed to the synergistic impact of mechanical deformation and heat during the FSW process, [14]. This leads to the refinement of grains and maybe the partial re-precipitation of hardening phases. Nevertheless, the hardness of this region remains lower than that of the basic metal, suggesting a certain level of softening. On the AA6061 side, the TMAZ exhibits a more significant decrease in hardness closer to the weld area. The concurrent effect of heat exposure and mechanical deformation in this area is expected to result in the dissolving of strengthening precipitates, which in turn leads to the observed decrease in hardness values [38]. The weld zone demonstrates the highest levels of hardness, 140 HV. The notable increase in hardness could be due to the vigorous plastic deformation and dynamic recrystallization that take place during the FSW process, resulting in a more refined grain structure. Similar findings on the FSW of AA2014 were observed by Wang et al. [39]. Moreover, the even distribution of reinforcing particles (Al_2O_3 and WC) within the weld zone leads to the increased hardness. The hardness of the weld zone exceeds that of the base metals, showing that the FSW technique significantly improves the mechanical qualities in this area.

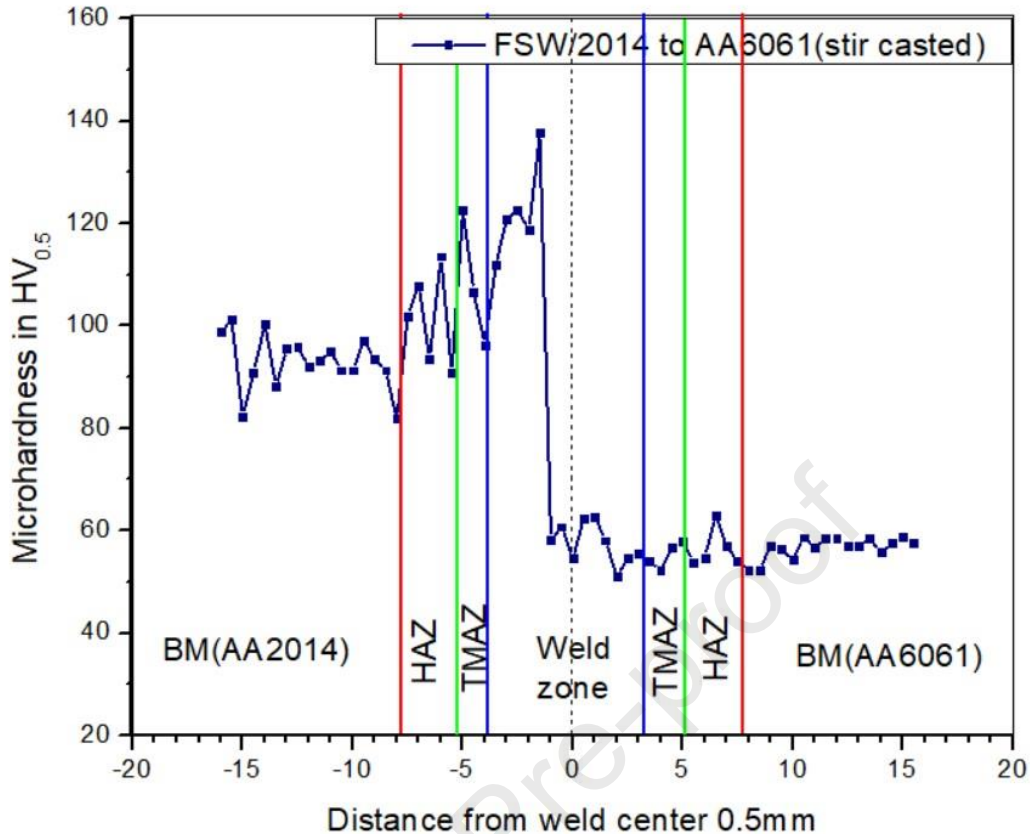


Fig. 8. The micro-hardness of the friction stir welded AAMMCs

3.7 Wear rate of the friction stir welded AAMMCs

The results of the wear test for the friction stir welded AAMMCs, as shown in Fig. 9, demonstrate the material's ability to resist wear, its frictional characteristics, and its overall durability under conditions involving friction and wear. These conditions are tested on test samples by measuring the friction coefficient, friction force and wear depth in microns. Figure 9(a) presents the total wear over time, demonstrating a steady and ongoing increase in wear depth. The linear trend is seen which illustrates a uniform retention for the given conditions, Bindhushree et al. [40]. The depth of wear is found to be 20 microns, indicating higher resistance to wear. Figure 9(b) exhibits a consistent value during the period of the test. The surface and contact interface of material with the surface remain in good condition throughout the test, as indicated by a consistent coefficient of friction, Mohrami et al. [41]. Figure 9(c) shows constant values throughout the experimental investigation with little variation. These variations can be related to the interaction between the roughnesses of the surfaces that are in contact. The presence of a consistent frictional force suggests that the surface roughness and hardness of the material create a constant barrier to sliding, hence reducing sudden fluctuations in frictional forces, Senthilraj et al. [42]. The consistent frictional force stability can be attributed to the ability of the reinforcing particles to endure the wear process, hence minimizing material loss and preserving contact integrity.

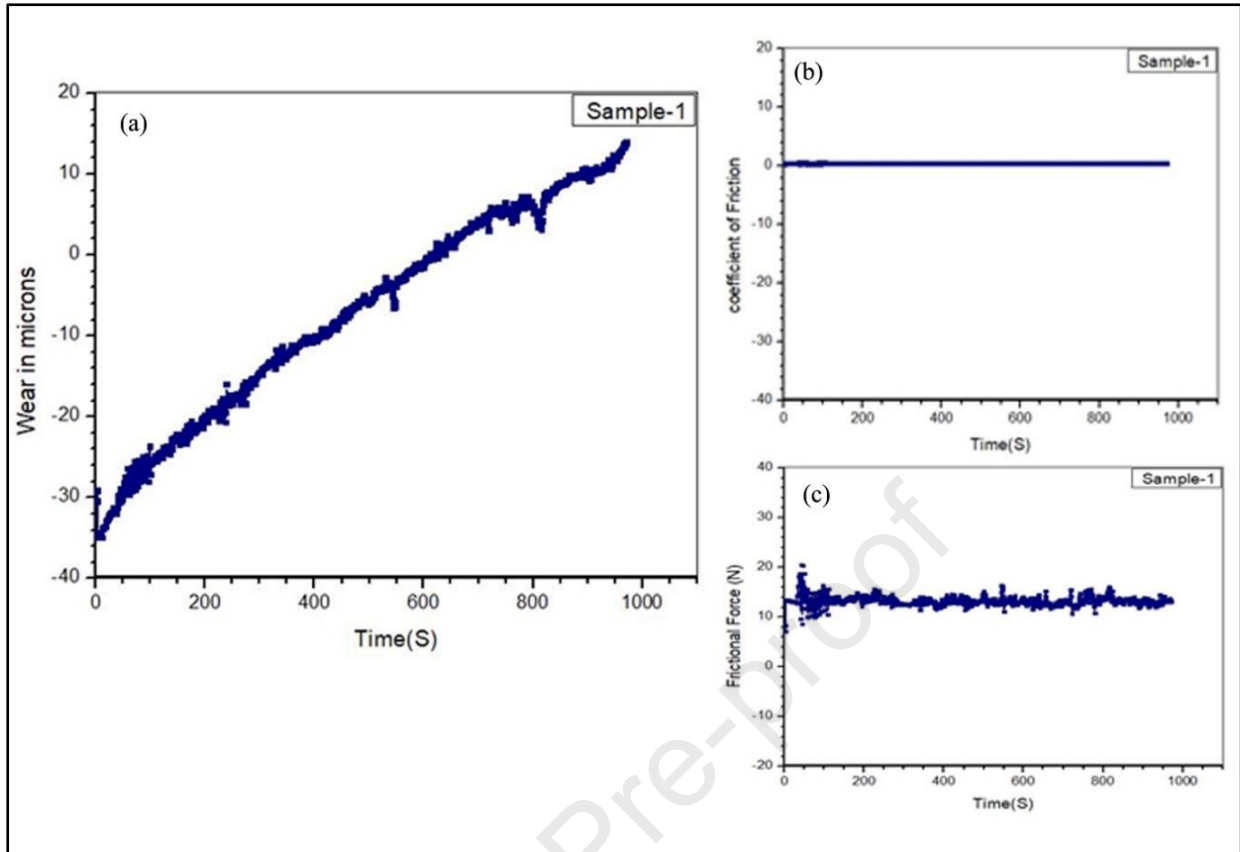


Fig. 9. (a) Wear Vs time, (b) Coefficient of friction Vs time and (c) Frictional force Vs time.

Furthermore, the microstructural homogenization, refined grain structure, and reduced elemental segregation has minimized localized galvanic effects and differential wear rates. The rationale for conducting the wear test is its assessment of the role of the mechanisms influencing particle dispersion, hardness gradients, and oxide layer stability in the processed material-load distribution, friction-induced deformation, and third-body abrasion.

3.8 Corrosion test results of friction stir welded AAMMCs

The results of the corrosion test for the friction stir welded AAMMCs are presented in Table 5. The corrosion potential (E_{corr}) is determined to be -1.308 V, reflecting the material's inclination to undergo corrosion. The relatively low value of E_{corr} indicates that the FSW joint is prone to corrosion in the specified environment, Afify et al. [43]. The corrosion current density (I_{corr}) is measured as 0.58 mA, and it is directly proportional to the rate at which the material deteriorates. A greater value of I_{corr} generally indicates a more rapid rate of corrosion, Zamrudi and Setiawan [44]. The pitting potential (E_{pit}) is determined to be -0.44 V, indicating the initiation of localized corrosion (pitting). The negative E_{pit} result indicates that the material is susceptible to pitting corrosion in the given test conditions [45]. The predicted overall corrosion rate is 0.0131563 mm/year, suggesting that the material undergoes a certain degree

of corrosion over time, although it is not extremely high. The polarization curve, as shown in Fig. 10, demonstrates the corrosion characteristics of the FSW of AAMMCs. The point at which the cathodic and anodic curves intersect, known as the corrosion potential, is estimated to be -1.308 V. The substantially negative number indicates that the FSW AAMMCs are susceptible to corrosion in the evaluated environment [46]. The decrease in E_{corr} relative to more corrosion-resistant materials suggests that the weld zone may be more prone to uniform corrosion. The cathodic node has a pronounced inclination, suggesting that the reduction reactions, possibly including hydrogen evolution, prevail at lower potentials. The anodic branch has a rather gradual incline at first, but it experiences a significant steepening with higher potentials. This pattern is a clear indication of localized corrosion processes, specifically pitting, which are frequently observed in Al alloys, particularly when exposed to chloride ions. The significant rise in current density at elevated potentials, found in the anodic branch, indicates the initiation of pitting corrosion, Zhang et al. [47]. The pitting potential (E_{pit}) is estimated to be -0.44 V, which is rather low, suggesting that the material is prone to pitting corrosion under the given test conditions. A greater I_{corr} value, as obtained in this test (0.58 mA), is indicative of a higher corrosion rate. This finding indicates that the FSW joint of AAMMCs may undergo substantial degradation over a period when subjected to comparable environmental conditions.

Table 5. The corrosion results of the friction stir welded AAMMCs

Alloy ID	E_{corr} (V)	I_{corr} (mA)	E_{pit} (V)	Corrosion Rate (mm.y^{-1})
AAMMC1 + AAMMC2	-1.308	0.58	-0.44	0.0131563

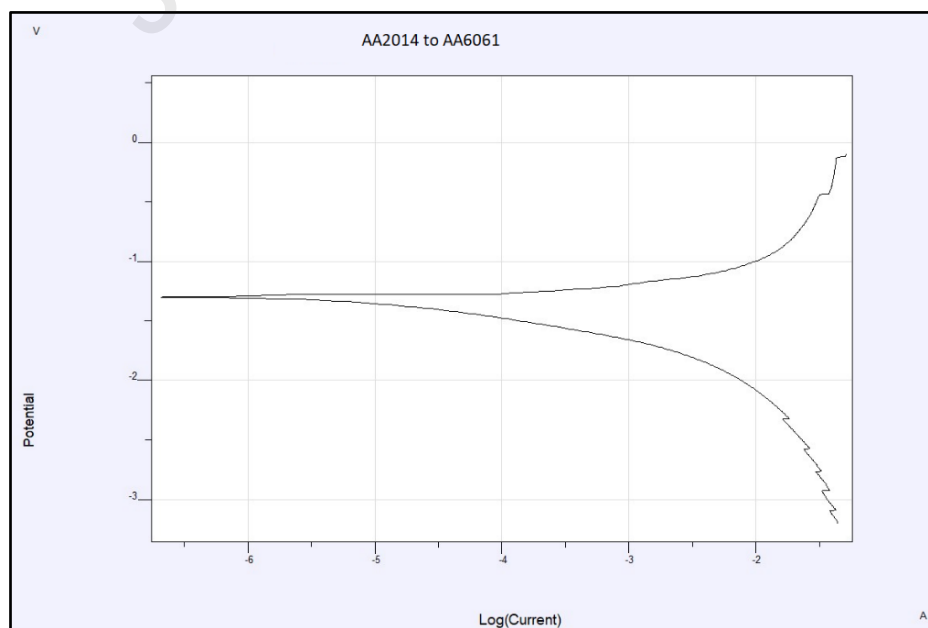


Fig. 10. The potential and log curves of friction stir welded AAMMCs

3.5 Macro and microstructures of friction stir welded AAMMCs

The friction stir welded AAMMCs were analyzed at both macro and microstructural levels, as shown in Fig. 11, to observe the structural changes that occurred in different areas such as the base metals (AA6061 and AA2014), the TMAZ on both sides, and the stir zone. Figure 11(a) shows that AA6061 base metal has a grain structure that is rather coarse, with elongated grains which indicates that the material is in a rolled condition. Similarly, Fig. 11(f) shows that AA2014 base metal exhibits a coarse, dendritic microstructure that is typical of cast Al alloys [13]. The existence of this rough formation in both base metals suggests that they have not undergone substantial modifications prior to the welding procedure, serving as a standard for evaluating the welded areas.

The TMAZ on both the AA6061 side, Fig. 11(b), and the AA2014 side, Fig. 11(e) exhibit significant alterations in microstructure because of the combined influence of heat and mechanical deformation during FSW. Figure 11(b) shows that the TMAZ on the AA6061 side has a more finely structured grain compared to the base metal, indicating some degree of partial recrystallization [48]. The grains show distortion along with stretching which indicates that the material has undergone plastic deformation. The AA2014 side, shown in Fig. 11(e), has a more refined and equi-axed grain structure compared to the coarser particles of the TMAZ base metal. The smaller grains in TMAZ suggest that temperature changes led to recrystallization, enhancing the mechanical properties in this specific area [36].

The stir zone is the region where the most substantial alterations in microstructure take place as a result of the high levels of plastic deformation and heat produced during FSW. The Fig. 11(c) shows a top stir zone with a well-developed and restructured grain structure, characterized by a consistent distribution of small, equi-axed grains. The observed structure is a distinctive feature of the dynamic recrystallization process that takes place during FSW, leading to a notable enhancement in mechanical properties, such as enhanced hardness and strength [49]. The refined grain structure is observed in the bottom stir zone of Fig. 11(d), with slightly larger grains compared to the top stir zone. The disparity may arise from fluctuations in the thermal dispersion and the speed at which the weld area cools [50]. The consistent grain structure throughout the stir zone suggests adequate mixing during FSW.

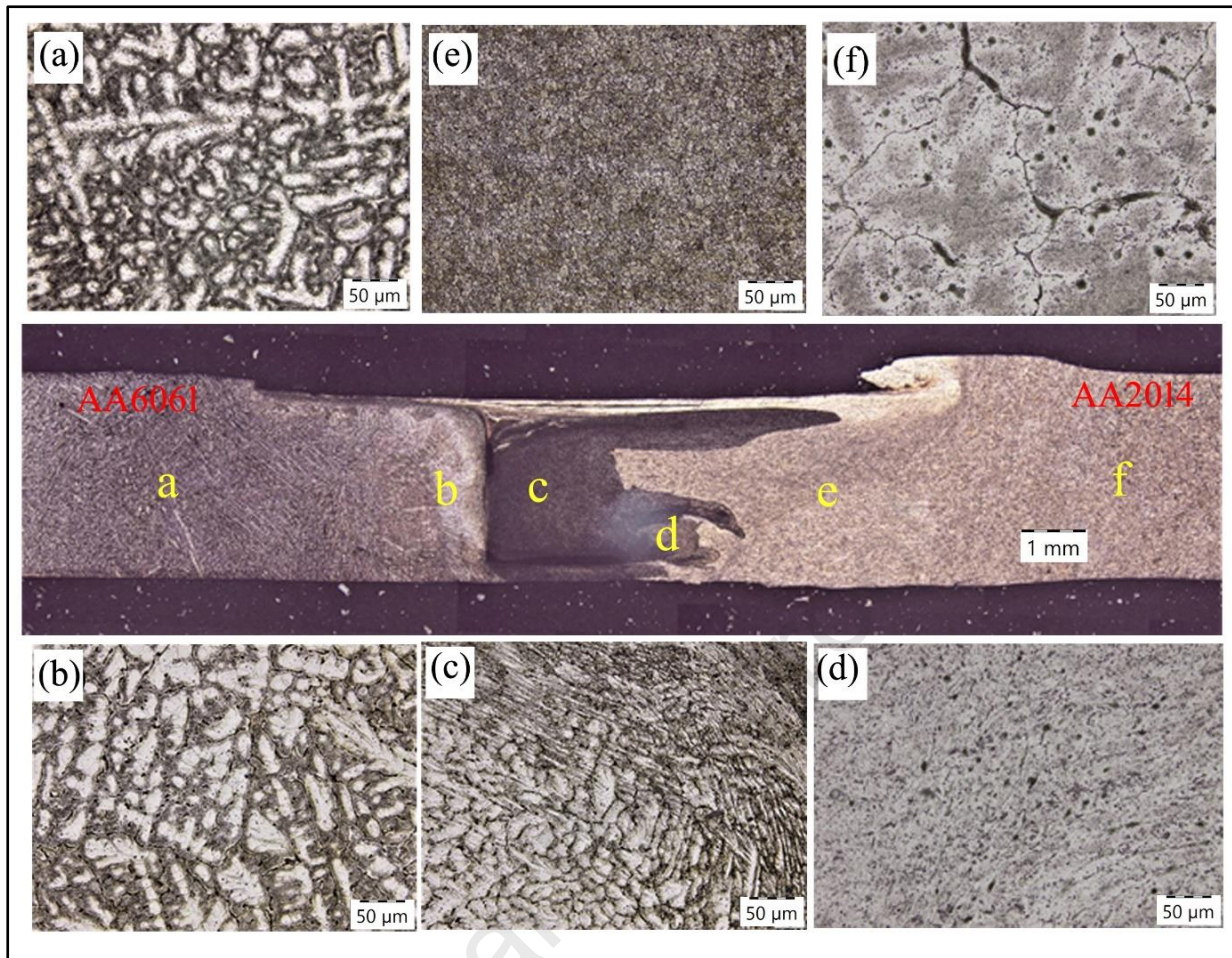


Fig. 11. Macro/microstructures of (a) Base metal AA6061, (b) TMAZ AA6061 side, (c) top nugget zone, (d) bottom nugget zone, (e) TMAZ AA2014 and (f) base metal AA2014

3.9 SEM analysis

The microstructure of the AA6061 base metal, as depicted in Fig. 12(a), shows a grain structure that is rather coarse, as is typical in the base metal prior to experiencing substantial plastic deformation. The microstructure exhibits a high degree of uniformity, with the presence of discernible second-phase particles, most likely precipitates, which significantly enhance the mechanical properties of the alloy [51]. The lack of substantial flaws suggests that the base material was in a satisfactory state prior to the welding process. Figure 12(b) illustrates the boundary between the TMAZ and the AA6061 base metal. The FSW process results in a notable reduction in the size of the microstructure in this area, which is attributed to the combined influence of heat and plastic deformation [52]. The grains next to the TMAZ exhibit elongation and deformation, which suggests the presence of mechanical agitation and a moderate level of recrystallization. The presence of smaller, more evenly spread particles indicates that the welding process improved the scattering of reinforcement particles, resulting in enhanced mechanical characteristics in this area [53].

The nugget top zone, depicted in Fig. 12(c), signifies the central region of the weld where the most significant plastic deformation and thermal exposure take place. The microstructure in this area is distinguished by a significantly finer grain structure, which is a consequence of dynamic recrystallization occurring during the FSW process [54]. The presence of small, evenly shaped grains in this area enhances the hardness and strength commonly observed in the nugget zone [55]. The even distribution of reinforcement particles in this area indicates that the stirring action of the FSW tool successfully spread the particles throughout the matrix, hence improving the overall mechanical properties of the joints. Figure 12(d) depicts the bottom zone of the nugget that has experienced substantial microstructural refinement. Nevertheless, the grains in this region exhibit a larger size compared to the grains in the upper zone, potentially attributed to variations in cooling rates or heat dispersion during the welding procedure. The homogeneous grain structure with dispersed particles in the bottom nugget zone suggests that it too experiences the strengthening effects of the FSW process [56-58].

As shown in Fig. 12(e), the interactions between TMAZ and AA2014 base metals exhibit a pattern of microstructural refinement similar to that reported for the AA6061 phase. The grains near the TMAZ on the AA2014 side are more refined than the base metal and the partial recrystallization is attributed to the heat and mechanical influences exerted by the FSW [36]. Figure 12(f) illustrate the microstructure of the AA2014 base metal with a coarse, dendritic structure. The microstructure exhibits a high degree of uniformity, characterized by prominent grains and discernible second-phase particles, which significantly enhance the alloy's intrinsic strength and hardness [59-61].

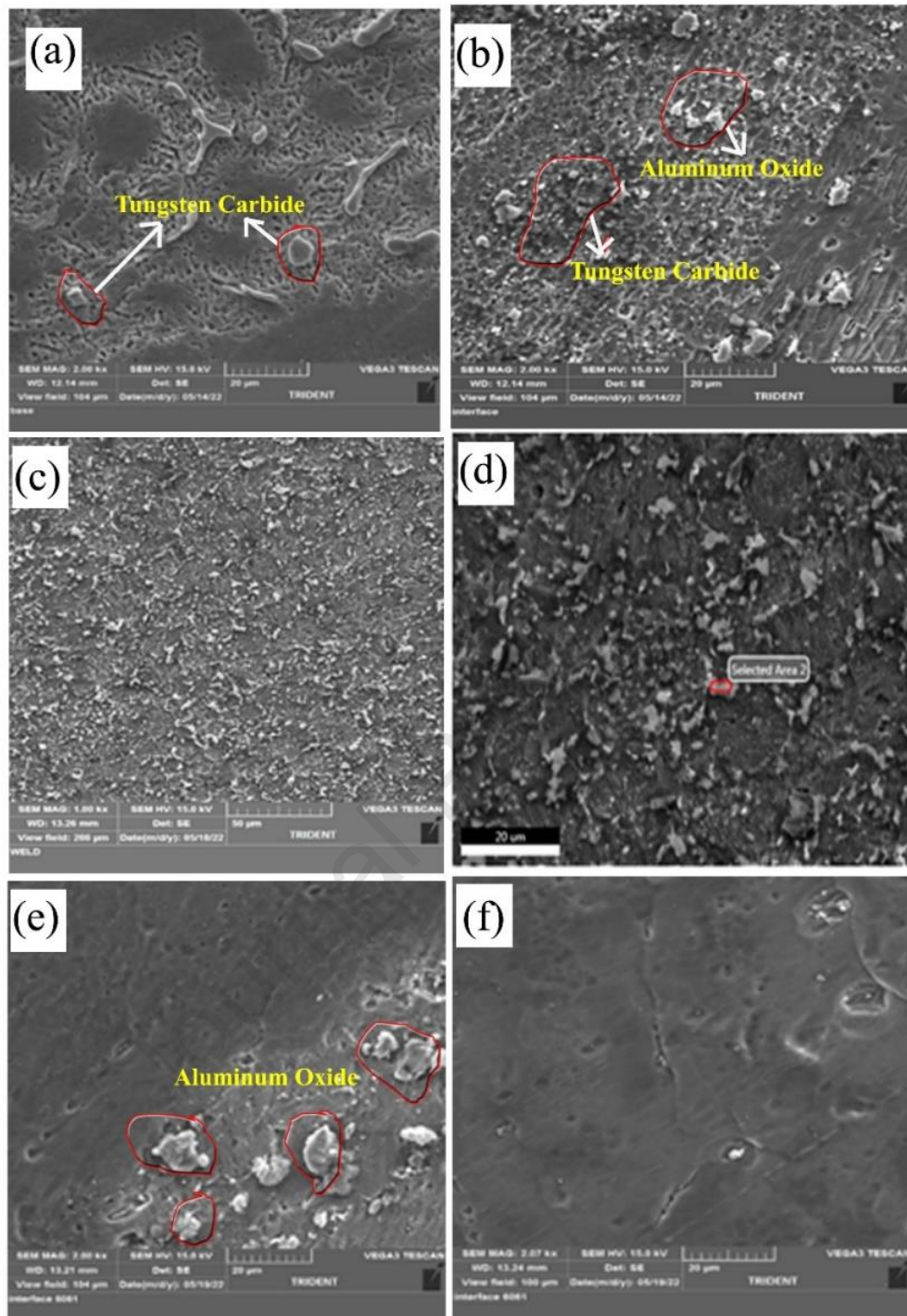


Fig. 12. (a) AA6061 base metal, (b) Interface left TMAZ AA6061 right, (c) Nugget top zone, (d) nugget bottom zone, (e) Interface left TMAZ AA2014 right and (f) AA2014 base metal

3.10 Energy Dispersive X- Ray Analysis

The EDX examination of different regions in the friction stir welded AAMMCs, as shown in Fig. 13, yields elemental composition data for the TMAZ of AA6061, the nugget zone and the TMAZ of AA2014. The EDS spectrum of the AA6061 TMAZ, Fig. 13(a), reveals the presence of Al, Cu, O₂ and Mg as the main detected elements. The prominent Al peak (Al K α 1) aligns

with the elemental composition of AA6061. The existence of O₂ suggests the existence of oxide phases, which are probably derived from the reinforcing particles (Al₂O₃) [55]. The presence of a Cu peak indicates that Cu is present in the TMAZ, which enhances the strength of the alloy. The FSW process has effectively maintained the consistency of the constituents of the material as indicated by the evenly distributed reinforcing particles over the TMAZ zone [62-64].

Fig. 13(b) illustrate the EDX spectrum of the nugget zone exhibits abundant Al, with prominent Cu, O₂ and Mg surfaces. The visible O₂ peak indicates a large fraction of oxides, probably due to the inclusion of Al₂O₃ and possibly WC. The presence of these oxides is essential for the stability and durability of the nugget zone. A noticeable peak in Cu indicates that Cu is spread evenly throughout the nugget area, which improves the overall strength [36]. The FSW process has effectively mixed the matrix as well as the reinforcement particles, producing a homogenized and reinforced nugget zone [65-67].

EDX analysis of TMAZ AA2014, Fig. 13(c), shows distinct peaks for Al, Cu, O₂ and Mg, similar to those observed in other regions. AA2014 is mainly made up of Al and Cu, with Cu being a key element that strengthens the material. The distribution of these elements in the TMAZ indicates that the FSW process effectively preserved the structural integrity of the material while mixing the reinforcement particles. The results from the EDX analysis of the AA2014 TMAZ align with those of the AA6061 TMAZ.

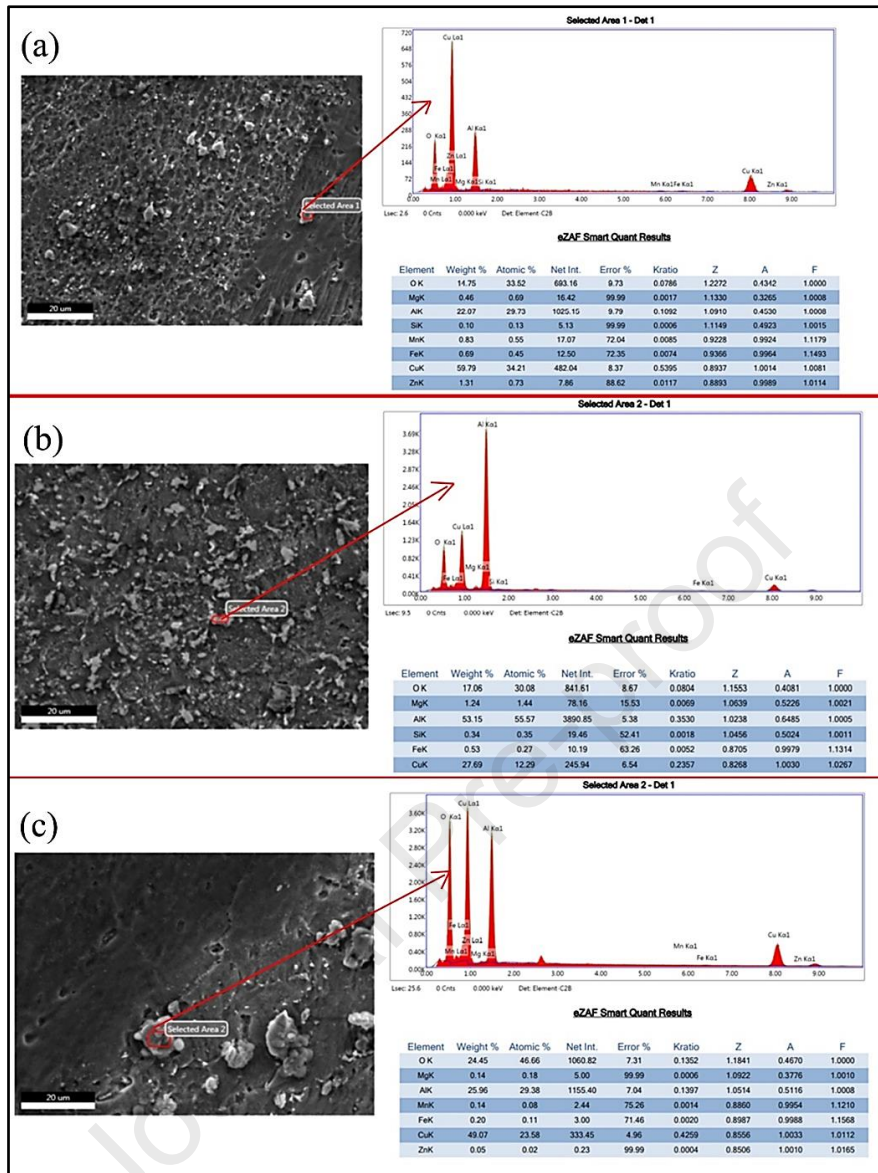


Fig. 13. (a) AA6061 TMAZ, (b) Nugget zone and (c) AA2024 TMAZ

Owing to their superior mechanical characteristics and enhanced performance in demanding industrial environments, the applications of stir casting and FSW with WC and Al₂O₃-based nano-particulates reinforced AA2024 and AA6061 aluminum alloys have attracted substantial interest. Stir casting, which is both cost-effective and efficient, is frequently implemented to fabricate Al-matrix composites that are reinforced with WC and Al₂O₃ nano-particles [68-70]. The nano-reinforcements are homogeneously dispersed through this process, resulting in composites that exhibit strengthened hardness, tensile strength, and resistance to abrasion [71-72]. Consequently, they are highly suitable for aerospace, automotive, and defense applications that require lightweight, high-strength materials [73-74]. The incorporation of WC and Al₂O₃ nano-particulates results in a rise in operational efficiency and a reduction in maintenance costs by prolonging the service lifespan of components including, engine-blocks, brake-rotors, and

aerospace structural frames [75-77]. This is accomplished by strengthening both hardness and resistance to wear.

Conversely, FSW has demonstrated outstanding potential in the welding of these advanced nano-reinforced Al-alloys without affecting their mechanical characteristics. In comparison to conventional fusion welding techniques, FSW facilitates the jointing of AA2014 and AA6061 alloys that are reinforced with ceramic particulates, resulting in welds that exhibit superior strength, resistance to corrosion, and fatigue performance [78-79]. This renders FSW a prospective technology for high-performance applications in industries including, construction, railway, and marine, where the development of resilient, robust, durable, and reliable welded-joint connections is essential [80]. The inclusion of nano-particulates further strengthens the thermostability and resistance to wear of FSW joints, thereby offering a novel emerging opportunities for their implementation in heavy-duty machinery and high-temperature environments [81].

Furthermore, the integration of FSW and stir casting offers a synergistic method for the production and joining of advanced Al-composites for critical applications in sectors including, energy, where high-efficiency, durable components are required. At the cutting-edge of material innovations, these technologies are positioned by their capacity to customize mechanical characteristics by precisely controlling the reinforcement-composition, and welding-parameters. The applications of WC and Al₂O₃ reinforced Al-alloys through stir casting and FSW represents a paradigm shift toward more resilient, lightweight, and environmentally friendly materials, ensuring significant advancements in modern engineering, as industries strives for more sustainable and high-performance solutions in Automotive, Aerospace, Defense, Marine, and Railway transportation sectors [82].

4. Conclusion

The mechanical properties, metallurgical studies, wear rate, and corrosion behavior of dissimilar weldments of AAMMCs reinforced with 5% Al₂O₃ and 5% WC particles have been extensively investigated in the current research work. AA2014 and AA6061 Al alloys have been taken under study that have initially been produced by the stir casting method followed by friction stir welding technique. Key results are discussed in the following sections;

- i.** The stir casting method was effectively used to produce AAMMCs with a consistent dispersion of reinforcement particles in the AA2014 and AA6061 matrices.
- ii.** The stir-cast composites showed tensile strengths of 155 MPa in AAMMC1 and micro-hardness of 116 HV due to the good integration of Al₂O₃ and WC particles in the reinforced composites.

- iii. The tensile strength of the AAMMCs joined through the FSW technique is found to be 156 MPa, showing reasonable weld strength along with enhanced hardness values at the TMAZ, which has been attributed to proper mechanical mixing assisted by the square tool pin profile.
- iv. The corrosion test shows that FSW joints obtained from stir casting possessed good resistance against corrosion; its rate stood at 0.0131563 mm/yr. From the wear test, it proved that the even dispersion of particles with reinforcement and proper microstructural integrity considerably improved both resistance against wear as well as against corrosion.
- v. The considerable strengthening of the composite structures was proven with the help of the addition of reinforcement particles into the Al matrix, further processed by the FSW method. SEM and EDS analysis showed defect-free AAMMC samples with uniformly distributed reinforcement within the TMAZ and nugget zone.

4.1 Limitations and Future Scope:

The study focuses on evaluation of corrosion resistance, wear rate, micro-hardness, welding strength, and changes in the microstructures & elemental analysis; however, the grain size distribution across different zones, essential for the detailed understanding of local mechanical properties, is not examined. The material also has not been tested under any fatigue loading condition. Future work will focus on analysing grain size in the weld zone and evaluating the fatigue behavior under cyclic loads to further enhance the understanding and applicability of these composites in practical conditions. In addition, the fractography analysis for the HAZ of Al6061 will be included in the future work.

Ethics declarations:

Conflict of Interests/Competing interests: The authors declare no competing interests.

Ethical approval: Not applicable.

Consent to participate: Not applicable.

Consent to publish: All authors have read and approved this manuscript.

Data availability statement: The data involved in the findings of the result will be shared by the corresponding author based on reasonable request.

Author Contributions: Conceptualization, Balram Yelamasetti, Chilakamarri L Aslesha, Vijaya Sarathi T, Rajyalakshmi G, Sagar Shelare, Shubham Sharma; Methodology, Balram Yelamasetti, Chilakamarri L Aslesha, Vijaya Sarathi T, Rajyalakshmi G, Sagar Shelare,

Shubham Sharma; Formal Analysis, Balram Yelamasetti, Chilakamarri L Aslesha, Vijaya Sarathi T, Rajyalakshmi G, Sagar Shelare, Shubham Sharma; Investigation, Balram Yelamasetti, Chilakamarri L Aslesha, Vijaya Sarathi T, Rajyalakshmi G, Sagar Shelare, Shubham Sharma; Writing—Original Draft Preparation, Balram Yelamasetti, Chilakamarri L Aslesha, Vijaya Sarathi T, Rajyalakshmi G, Sagar Shelare, Shubham Sharma; Writing—Review And Editing, Shubham Sharma, Karthikeyan A, AI Ismail; Supervision, Shubham Sharma, Karthikeyan A, AI Ismail; Project Administration, Shubham Sharma, Karthikeyan A, AI Ismail; Funding Acquisition, Shubham Sharma, Karthikeyan A, AI Ismail. All authors have read and agreed to the published version of the manuscript.

Funding: This research work was funded by Umm-Alqura University, Saudi Arabia under grant number: 25UQU4240002GSSR01NI.

Acknowledgments: This research work was funded by Umm-Alqura University, Saudi Arabia under grant number: 25UQU4240002GSSR01NI.

Conflicts of Interest: The authors declare no conflict of interest.

References

1. Polayya C, Rao CS, Kumar GV. Improving the properties of aluminum-lithium composites in aerospace applications. *Engineering Research Express*. 2024; 6(2): 022501. <https://doi.org/10.1088/2631-8695/ad3a37>
2. Derbiszewski B, Obraniak A, Rylski A, Siczek K, Wozniak M. Studies on the Quality of Joints and Phenomena Therein for Welded Automotive Components Made of Aluminum Alloy—A Review. *Coatings*. 2024; 14(5): 601. <https://doi.org/10.3390/coatings14050601>
3. Veeresh Kumar, G. B., et al. "Effect of tungsten carbide reinforcement on the aluminum 6061 alloy." *Journal of Testing and Evaluation* 47.4 (2019): 2613-2629. <https://doi.org/10.1520/JTE20170545>
4. Deep, BN Akash, et al. "Ultrasonic assisted stir squeeze casting of AA5456/Al₂O₃-SiC-Gr-MoS₂ hybrid nanocomposites: Microstructure and strengthening analysis." *Journal of Materials Research and Technology* 34 (2025): 1611-1635. <https://doi.org/10.1016/j.jmrt.2024.12.172>
5. Yi, Jiang-long, et al. "Reinforcing effects of nano-WC in AlSi10Mg alloy assisted by in-situ surface modification approach." *Transactions of Nonferrous Metals Society of China* 34.1 (2024): 50-64. [https://doi.org/10.1016/S1003-6326\(23\)66381-2](https://doi.org/10.1016/S1003-6326(23)66381-2)
6. Kashaev N, Ventzke V, Çam G. Prospects of laser beam welding and friction stir welding processes for aluminum airframe structural applications. *Journal of Manufacturing Processes*. 2018; 36: 571-600. <https://doi.org/10.1016/j.jmapro.2018.10.005>

7. Ramana GV, Yelamasetti B, Vardhan TV. Effect of FSW process parameters and tool profile on mechanical properties of AA 5082 and AA 6061 welds. *Materials Today: Proceedings*. 2021; 46: 826-830. <https://doi.org/10.1016/j.matpr.2020.12.801>
8. Kumar R, Upadhyay V, Pandey C. Effect of post-weld heat treatments on microstructure and mechanical properties of friction stir welding joints of AA2014 and AA7075. *Journal of Materials Engineering and Performance*. 2023; 32(24): 10989-10999. <https://doi.org/10.1007/s11665-023-07927-0>
9. Yelamasetti, B., Kumar, P. N., Ramana G, V., Kumar Saxena, K., Singh, D., Kang, A. S., & Mohammed, K. A. (2023). Wear and corrosion behaviour of multiple pass friction stir processing on aluminium alloy 6061 embedding with B4C particles. *Advances in Materials and Processing Technologies*, 10(2), 531–540. <https://doi.org/10.1080/2374068X.2023.2171667>
10. Yelamasetti, B., Kumar, P. N., Venkat Ramana, G., Saxena, K. K., Msomi, V., Vishwanatha, H. M., & Behera, A. (2022). Surface modification of aluminum alloy 6061 by embedding B4C particles via friction stir processing. *Materials Research Express*, 9(5). <https://doi.org/10.1088/2053-1591/ac6da7>
11. Xavier JF, Rajendran C, Sivamaran V, Mandal TK. Characterization of material flow behavior in friction stir welded AA2014 aluminum alloy joints. *Materials Testing*. 2024. <https://doi.org/10.1515/mt-2023-0370>
12. Kannaiyan S, Murugesan S, Thirumalaikannan D, Visvalingam B, Nagasai BP. Characteristics analysis and monitoring of friction stir welded dissimilar AA5083/AA6061-T6 using acoustic emission technique. *Welding International*. 2024: 1-8. <https://doi.org/10.1080/09507116.2024.2376187>
13. Bindhushree BS, Sevel P, Shanmuganatan SP, Saravanabavan D, Madhusudan M. Influence of tool geometry on mechanical and microstructural characteristics of friction stir welded cast alloys. *Practical Metallography*. 2024; 61(5): 292-318. <https://doi.org/10.1515/pm-2023-1055>
14. Rana R, Karunakar DB, Karmakar A, Mathew T. Comparative Analysis of Microstructure Evolution and Mechanical Properties of Dissimilar Welded Joints of AA7075/AA6061 via Friction Stir Welding, Tungsten Inert Gas Welding, and Tungsten Inert Gas+ Friction Stir Processing. *Journal of Materials Engineering and Performance*. 2024. <https://doi.org/10.1007/s11665-024-09442-2>
15. Kar A, Singh K, Kumar L. Effect of tool rotational speed and mechanisms associated with microstructure evolution and intermetallics formation in friction stir welding of aluminum alloy to titanium alloy. *Journal of Materials Engineering and Performance*. 2024; 33(13): 6748-6759. <https://doi.org/10.1007/s11665-023-08407-1>
16. Zhu X, Wang R, Wang L, Liu M, Li S. Effect of Rotational Shear and Heat Input on the Microstructure and Mechanical Properties of Large-Diameter 6061 Aluminium Alloy

- Additive Friction Stir Deposition. *Crystals*. 2024; 14(7): 581. <https://doi.org/10.3390/cryst14070581>
17. Wang Z, Yang L, Chen S, Gao Y, Yu J. Investigation of temperature distribution, microstructure evolution, and weld performance in stir friction welded joints of 6061 aluminum alloys. *The International Journal of Advanced Manufacturing Technology*. 2024; 132, 4559–4583. <https://doi.org/10.1007/s00170-024-13557-0>
 18. Sabry I, Singh VP, Alkhedher M, El-Zathry NE, Mourad AH, Naseri M. Effect of rotational speed and penetration depth on Al-Mg-Si welded T-joints through underwater and conventional friction stir welding. *Journal of Advanced Joining Processes*. 2024; 9: 100207. <https://doi.org/10.1016/j.jajp.2024.100207>
 19. Essa AR, Eldersy RI, Ahmed MM, Abd El-Aty A, Alamry A, Alzahrani B, El-Nikhaily AE, Habba MI. Modeling and experimental investigation of the impact of the hemispherical tool on heat generation and tensile properties of dissimilar friction stir welded AA5083 and AA7075 Al alloys. *Materials*. 2024; 17(2): 433. <https://doi.org/10.3390/ma17020433>
 20. Tobin D, O'Shaughnessy S, Trimble D. Characterisation of force and torque with auxiliary heating during friction stir spot welding of AA2024-T3. *Results in Materials*. 2024; 21: 100535. <https://doi.org/10.1016/j.rinma.2024.100535>
 21. de Queiroz Caetano G, Andrade TC, Motta MF, Miranda HC, Farias JP, Bergmann LA, dos Santos JF, Silva CC. Assessment of the joint configuration and welding parameters for the dissimilar joining of AISI 304 L and AISI 410S stainless steels by friction stir welding. *The International Journal of Advanced Manufacturing Technology*. 2024. <https://doi.org/10.1007/s00170-024-14071-z>
 22. Li, Yuan, et al. "Microstructure and mechanical properties of ultrasonic spot welding of AA7075-T6 and A380 casting aluminum alloy." *Journal of Manufacturing Processes* 110 (2024): 126-133. <https://doi.org/10.1016/j.jmapro.2023.12.061>
 23. Sun, Kelun, et al. "Influence of ZrB₂ and Al₂O₃ nanoparticles on microstructure and mechanical property of friction stir welded joints of in-situ 7085Al matrix composites." *Journal of Materials Processing Technology* 326 (2024): 118323. <https://doi.org/10.1016/j.jmatprotec.2024.118323>
 24. Parikh VK, Badgujar AD, Ghetiya ND. Investigation of microstructural and wear properties of stir cast and friction stir processed AA 2014-based metal matrix composites. *Advances in Materials and Processing Technologies*. 2023; 9(4): 1920-1940. <https://doi.org/10.1080/2374068X.2022.2136688>
 25. Molla Ramezani N, Davoodi B. Evaluating the influence of various friction stir processing strategies on surface integrity of hybrid nanocomposite Al6061. *Scientific Reports*. 2024; 14(1): 8056. <https://doi.org/10.1038/s41598-024-58714-3>
 26. Kumar J, Kumar G, Mehdi H, Kumar M. Optimization of FSW parameters on mechanical properties of different aluminum alloys of AA6082 and AA7050 by response surface

- methodology. *International Journal on Interactive Design and Manufacturing (IJIDeM)*. 2024; 18(3): 1359-1371. <https://doi.org/10.1007/s12008-023-01425-2>
27. Gadakh VS, Kumar A. Modelling and microstructure of friction stir welds of AA2014 alloy: Different tool pin profiles. *Materials Today: Proceedings*. 2018; 5(2): 7447-7456. <https://doi.org/10.1016/j.matpr.2017.11.416>
28. Uday KN, Rajamurugan G. Influence of process parameters and its effects on friction stir welding of dissimilar aluminium alloy and its composites—a review. *Journal of Adhesion Science and Technology*. 2023; 37(5): 767-800. <https://doi.org/10.1080/01694243.2022.2053348>
29. Jenarathanan MP, Varma CV, Manohar VK. Impact of friction stir welding (FSW) process parameters on tensile strength during dissimilar welds of AA2014 and AA6061. *Materials Today: Proceedings*. 2018; 5(6): 14384-14391. <https://doi.org/10.1016/j.matpr.2018.03.023>
30. Gaurav S, Mishra RS, Zunaid M. Enhancement of microstructure and mechanical properties of similar and dissimilar aluminium alloy by friction stir welding/processing using nanoparticles: a review. *Journal of Adhesion Science and Technology*. 2023; 37(22): 3125-3166. <https://doi.org/10.1080/01694243.2023.2186756>
31. Abioye TE, Zuhailawati H, Anasyida AS, Ayodeji SP, Oke PK. Effects of particulate reinforcements on the hardness, impact and tensile strengths of AA 6061-T6 friction stir weldments. *Proceedings of the Institution of Mechanical Engineers, Part L: Journal of Materials: Design and Applications*. 2021; 235(6): 1500-1506. <https://doi.org/10.1177/1464420721995544>
32. Nagaraja S, Anand PB, Mariswamy M, Alkahtani MQ, Islam S, Khan MA, Khan WA, Bhutto JK. Friction stir welding of dissimilar Al–Mg alloys for aerospace applications: Prospects and future potential. *Reviews on Advanced Materials Science*. 2024; 63(1): 20240033. <https://doi.org/10.1515/rams-2024-0033>
33. Kumar RA, Thansekhar MR. Reinforcement with alumina particles at the interface region of AA6101-T6 and AA1350 alloys during friction stir welding. *Materials Research Express*. 2018; 5(4): 046521. <https://doi.org/10.1088/2053-1591/aab8b5>
34. Maji P, Ghosh SK, Nath RK, Karmakar R. Microstructural, mechanical and wear characteristics of aluminum matrix composites fabricated by friction stir processing. *Journal of the Brazilian Society of Mechanical Sciences and Engineering*. 2020; 42: 191. <https://doi.org/10.1007/s40430-020-02279-5>
35. Raturi M, Garg A, Bhattacharya A. Tensile strength and failure of dissimilar friction stir welded joints between 6061-T6 and 2014-T6 aluminum alloys. *Procedia Structural Integrity*. 2019; 17: 495-502. <https://doi.org/10.1016/j.prostr.2019.08.065>
36. Mohan AE, Sajuri Z, Baghdadi AH, Abbasi M. Influences of Graphene Nanoplatelet Addition and Pin Lengths on the Microstructure and Mechanical Properties of 7075

- Aluminum Alloy Under Friction Stir Spot Welding. *Journal of Materials Research and Technology*. 2024; 31: 3436-3452. <https://doi.org/10.1016/j.jmrt.2024.07.065>
37. Abdollahzadeh A, Bagheri B, Abassi M, Kokabi AH, Moghaddam AO. Comparison of the weldability of AA6061-T6 joint under different friction stir welding conditions. *Journal of Materials Engineering and Performance*. 2021; 30: 1110-1127. <https://doi.org/10.1007/s11665-020-05379-4>
 38. Singh VP, Patel SK, Kuriachen B. Mechanical and microstructural properties evolutions of various alloys welded through cooling assisted friction-stir welding: A review. *Intermetallics*. 2021; 133: 107122. <https://doi.org/10.1016/j.intermet.2021.107122>
 39. Wang S, Wei X, Xu J, Hong J, Song X, Yu C, Chen J, Chen X, Lu H. Strengthening and toughening mechanisms in refilled friction stir spot welding of AA2014 aluminum alloy reinforced by graphene nanosheets. *Materials & Design*. 2020; 186: 108212. <https://doi.org/10.1016/j.matdes.2019.108212>
 40. Bindhushree BS, Shanmuganatan SP, Madhusudan M, Saravanabavan D. Experimental Investigation on Wear and Corrosion behavior of stir cast alloys and friction stir cast welds. *Journal of Bio-and Tribo-Corrosion*. 2024; 10(3): 60. <https://doi.org/10.1007/s40735-024-00862-0>
 41. Moharami A, Razaghian A, Babaei B, Ojo OO, Šlapáková M. Role of Mg₂Si particles on mechanical, wear, and corrosion behaviors of friction stir welding of AA6061-T6 and Al-Mg₂Si composite. *Journal of Composite Materials*. 2020; 54(26): 4035-4057. <https://doi.org/10.1177/0021998320925528>
 42. Senthilraj K, Rajamurugan G. Impact of friction stir welding parameters and Al₂TiO₅ reinforcement on the mechanical, wear, and corrosion performance of dissimilar welded aluminium composite joints. *Journal of Adhesion Science and Technology*. 2024. <https://doi.org/10.1080/01694243.2024.2331479>
 43. Afify R, Gamil M. Effect of welding settings on mechanical characteristics, microstructural features, and corrosion performance in friction stir welding of dissimilar AA6082-T6/7075-T6 joints. *Journal of Al-Azhar University Engineering Sector*. 2024; 19(71): 677-697. <https://doi.org/10.21608/aej.2024.265883.1605>
 44. Zamrudi FH, Setiawan AR. Effect of friction stir welding parameters on corrosion behaviour of aluminium alloys: an overview. *Corrosion Engineering, Science and Technology*. 2022; 57(7): 696-707. <https://doi.org/10.1080/1478422X.2022.2116185>
 45. Rajnaveen B, Rambabu G, Prakash K, Rao KS. Establishing optimal friction stir welding parameters for AA2219-T87 Al-alloy using comprehensive RSM and GA approach. *Engineering Research Express*. 2021; 3(4): 045054. <https://doi.org/10.1088/2631-8695/ac41b5>
 46. Sinhmar S, Dwivedi DK. A study on corrosion behavior of friction stir welded and tungsten inert gas welded AA2014 aluminium alloy. *Corrosion Science*. 2018; 133: 25-35. <https://doi.org/10.1016/j.corsci.2018.01.012>

47. Zhang C, Huang G, Cao Y, Li Q, Zhu Y, Huang X, Liu Q. Investigation on microstructure and localized corrosion behavior in the stir zone of dissimilar friction-stir-welded AA2024/7075 joint. *Journal of Materials Science*. 2020; 55: 15005-15032. <https://doi.org/10.1007/s10853-020-05072-w>
48. Madhusudan M, Shanmuganatan SP, Shridhar K, John J, Krishnamurthy R, Sasikumar B. Investigation on Friction Stir Weldability Characteristics of AA7075-T651 and AA6061-T6 Based Nanocomposites. *Advances in Materials Science and Engineering*. 2021; 2021(1): 3536353. <https://doi.org/10.1155/2021/3536353>
49. Tao W, Shuwei D, Matsuda K, Yong Z. Dynamic recrystallization and dynamic precipitation in AA6061 aluminum alloy during friction stir welding. *Transactions of the Indian Institute of Metals*. 2022; 75(5): 1329-1339. <https://doi.org/10.1007/s12666-021-02490-5>
50. Chinnasamy R, Srinivasan K, Balasubramanian V, Balaji H, Vinoth Kumar M, Raguathan S. Dynamic recrystallization in friction stir welded AA2014 aluminium alloy joints to replace riveted joints. *Materials Testing*. 2023; 65(7): 1085-1096. <https://doi.org/10.1515/mt-2022-0351>
51. Ghosh B, Das H, Samanta A, Majumdar JD, Ghosh M. Influence of tool rotational speed on the evolution of microstructure and mechanical properties of precipitation-hardened Aluminium 6061 butt joint during friction stir welding. *Engineering Research Express*. 2022; 4(1): 015009. <https://doi.org/10.1088/2631-8695/ac4a48>
52. Ahmed MM, El-Sayed Seleman MM, Fydrych D, Çam G. Friction stir welding of aluminum in the aerospace industry: the current progress and state-of-the-art review. *Materials*. 2023; 16(8): 2971. <https://doi.org/10.3390/ma16082971>
53. Zhang H, Zhang B, Gao Q, Song J, Han G. A review on microstructures and properties of graphene-reinforced aluminum matrix composites fabricated by friction stir processing. *Journal of Manufacturing Processes*. 2021; 68: 126-135. <https://doi.org/10.1016/j.jmapro.2021.07.023>
54. Mamgain A, Singh V, Pratap Singh A. Influence of welding parameters on mechanical property during friction stir welded joint on aluminium alloys: a review. *J. Kejuruter*. 2023; 35(1): 13-28. [https://doi.org/10.17576/jkukm-2023-35\(1\)-02](https://doi.org/10.17576/jkukm-2023-35(1)-02)
55. Saravanan V, Banerjee N, Amuthakkannan R, Rajakumar S. Microstructural evolution and mechanical properties of friction stir welded dissimilar AA2014-T6 and AA7075-T6 aluminum alloy joints. *Metallography, Microstructure, and Analysis*. 2015; 4: 178-187. <https://doi.org/10.1007/s13632-015-0199-z>
56. Ji, Renjie, Qingyang Zhao, Lilong Zhao, Yonghong Liu, Hui Jin, Lixin Wang, Lujun Wu, and Zhiqian Xu. "Study on high wear resistance surface texture of electrical discharge machining based on a new water-in-oil working fluid." *Tribology International* 180 (2023): 108218.

57. Yang, M. L., J. L. Xu, J. Huang, L. W. Zhang, and J. M. Luo. "Wear resistance of N-doped CoCrFeNiMn high entropy alloy coating on the Ti-6Al-4V alloy." *Journal of Thermal Spray Technology* (2024): 1-11.
58. Hu, Z., Zheng, J., Hua, L. and Sun, Q., 2024. Investigation of forging formability, microstructures and mechanical properties of pre-hardening Al-Zn-Mg-Cu alloy. *Journal of Manufacturing Processes*, 131, pp.2082-2100.
59. Zhang, M., Paidar, M., Ojo, O.O., Mehrez, S., Narayanasamy, S., Zain, A.M. and Mohanavel, V., 2022. Impact of multiple FSP passes on structure, mechanical, tribological and corrosion behaviors of AA6061/316 stainless-steel reinforced Al matrix composites. *Surface and Coatings Technology*, 447, p.128801.
60. Liu, S., Paidar, M., Ojo, O.O., Poková, M.Š., Mehrez, S., Zain, A.M., Zhao, Q. and Wang, J., 2023. Friction stir processing of hybridized AZ31B magnesium alloy-based composites by adding CeO₂ and ZrO₂ powders: mechanical, wear, and corrosion behaviors. *Journal of Materials Research and Technology*, 24, pp.1949-1972.
61. S. P. Dwivedi and S. Sharma, "Development and characterization of Cu-Ni-Al₂O₃ surface composite developed by friction stir process technique," *Mater. Today Commun.*, vol. 37, 2023, Art. no. 107399. <https://doi.org/10.1016/j.mtcomm.2023.107399>.
62. S. P. Dwivedi and S. Sharma, "Effect of CeO₂-Ni addition on the behavior of AZ91-A356 based composite fabricated by friction solid state technique," *Mater. Chem. Phys.*, vol. 311, 2024, Art. no. 128551. <https://doi.org/10.1016/j.matchemphys.2023.128551>.
63. S. Dwivedi, et al., "Alumina catalyst waste utilization for aluminum-based composites using the friction stir process," *Mater. Test.*, vol. 64, no. 4, pp. 533-540, 2022. <https://doi.org/10.1515/mt-2021-2074>.
64. S. P. Dwivedi and S. Sharma, "Effect of Ni addition on the behavior of dissimilar A356-AZ91/CeO₂ aluminum-magnesium based composite fabricated by friction stir process technique," *Compos. Interfaces*, vol. 31, no. 3, pp. 305-330, 2024. <https://doi.org/10.1080/09276440.2023.2260236>.
65. S. P. Dwivedi, R. Agrawal, and S. Sharma, "Effect of friction stir process parameters on mechanical properties of chrome containing leather waste reinforced aluminium based composite," *Int. J. Precis. Eng. Manuf.-Green Technol.*, vol. 8, pp. 935-943, 2021. <https://doi.org/10.1007/s40684-021-00312-z>.
66. S.P. Dwivedi, et al., "Exploring microstructural, interfacial, mechanical, and wear properties of AlSi7Mg0.3 composites with TiMOVWCr high-entropy alloy powder," *ACS Omega*, vol. 9, no. 17, pp. 18813-18826, 2024. <https://doi.org/10.1021/acsomega.3c07837>.
67. S. Sharma, S. P. Dwivedi, K. A. Mohammed, et al., "Investigation of surface hardness, thermostability, tribo-corrosion, and microstructural morphological properties of microwave-synthesized high entropy alloy FeCoNiMnCu coating claddings on steel," *Sci. Rep.*, vol. 14, p. 5160, 2024. <https://doi.org/10.1038/s41598-024-55331-y>.

68. S. P. Dwivedi, S. Sharma, and A. Singh, "Tailoring AlSi7Mg0.3 composite properties with CoCrMoNbTi high entropy alloy particles addition via FSP technique," *Mater. Chem. Phys.*, 2024, Art. no. 129038. <https://doi.org/10.1016/j.matchemphys.2024.129038>.
69. S. P. Dwivedi and S. Sharma, "Synthesis of high entropy alloy AlCoCrFeNiCuSn reinforced AlSi7Mg0.3 based composite developed by solid state technique," *Mater. Lett.*, vol. 355, 2024, Art. no. 135556. <https://doi.org/10.1016/j.matlet.2023.135556>.
70. S. Sharma, et al., "Physicomechanical, wettability, corrosion, thermal, and microstructural morphology characteristics of carbonized and uncarbonized bagasse ash waste-reinforced Al-0.45 Mg-0.35 Fe-0.25 Si-based composites: fabrications and characterizations," *ACS Omega*, vol. 9, no. 17, pp. 18836–18853, 2024. <https://doi.org/10.1021/acsomega.3c08109>.
71. B. Singh, et al., "Tribomechanical, and microstructural morphological analysis of nitride ferrous powder metallurgy composites for enhanced automotive valve guide performance," *J. Mater. Res. Technol.*, pp. 1–21, 2024. <https://doi.org/10.1016/j.jmrt.2024.06.001>.
72. G. Rajkumar, et al., "Parametric optimization of powder-mixed EDM of AA2014/Si3N4/Mg/cenosphere hybrid composites using fuzzy Logic: analysis of mechanical, machining, microstructural, and morphological characterizations," *J. Compos. Sci.*, vol. 7, p. 380, 2023. <https://doi.org/10.3390/jcs7090380>.
73. S. P. Dwivedi, V. Chaudhary, S. Sharma, and S. Sharma, "Ultrasonic vibration effect in the development of Al/CCLW/alumina metal matrix composite to enhance mechanical properties," *Proc. Inst. Mech. Eng., Part E*, pp. 1–14, 2023. <https://doi.org/10.1177/095444089231200467>.
74. K. Raman, et al., "Exploring the intricacies of machine learning-based optimization of electric discharge machining on squeeze cast TiB2/AA6061 composites: insights from morphological, and microstructural aspects in the surface structure analysis of recast layer formation and worn-out analysis," *J. Mater. Res. Technol.*, vol. 26, pp. 8569–8603, 2023. <https://doi.org/10.1016/j.jmrt.2023.09.127>.
75. S. Dwivedi, et al., "Heat treatment behavior of Cr in the form of collagen powder and Al₂O₃ reinforced aluminum-based composite material," *J. Mater. Res. Technol.*, vol. 25, pp. 3847–3864, 2023. <https://doi.org/10.1016/j.jmrt.2023.06.203>.
76. J. Kumar, et al., "Comparative study on the mechanical, tribological, morphological and structural properties of vortex casting processed, Al–SiC–Cr hybrid metal matrix composites for high strength wear-resistant applications: fabrication and characterizations," *J. Mater. Res. Technol.*, vol. 9, pp. 13607–13615, 2020. <https://doi.org/10.1016/j.jmrt.2020.10.001>.
77. J. Kumar, et al., "Investigation on the mechanical, tribological, morphological and machinability behavior of stir-casted Al/SiC/Mo reinforced MMCs," *J. Mater. Res. Technol.*, vol. 12, pp. 930–946, 2021. <https://doi.org/10.1016/j.jmrt.2021.03.034>.
78. J. Kumar, S. Sharma, J. Singh, S. Singh, and G. Singh, "Optimization of wire-EDM process parameters for Al-Mg-0.6Si-0.35Fe/15%RHA/5%Cu hybrid metal matrix composite using

- TOPSIS: processing and characterizations,” *J. Manuf. Mater. Process.*, vol. 6, p. 150, 2022. <https://doi.org/10.3390/jmmp6060150>.
79. H. K. Garg, et al., “Multi-objective parametric optimization on the EDM machining of hybrid SiCp/Grp/aluminum nanocomposites using Non-dominating Sorting Genetic Algorithm (NSGA-II): fabrication and microstructural characterizations,” *Rev. Adv. Mater. Sci.*, vol. 61, pp. 931–953, 2022. <https://doi.org/10.1515/rams-2022-0279>.
80. S. Sharma, et al., “Investigation on mechanical, tribological and microstructural properties of Al–Mg–Si–T6/SiC/muscovite-hybrid metal-matrix composites for high strength applications,” *J. Mater. Res. Technol.*, vol. 12, pp. 1564–1581, 2021. <https://doi.org/10.1016/j.jmrt.2021.03.095>.
81. S. Sharma, V. Patyal, P. Sudhakara, J. Singh, M. Petru, and R. A. Ilyas, “Mechanical, morphological, and fracture-deformation behavior of MWCNTs-reinforced (Al–Cu–Mg–T351) alloy cast nanocomposites fabricated by optimized mechanical milling and powder metallurgy techniques,” *Nanotechnol. Rev.*, vol. 11, pp. 65–85, 2021. <https://doi.org/10.1515/ntrev-2022-0005>.
82. R. Kumar, et al., “Effect of particle size and weight fraction of SiC on the mechanical, tribological, morphological, and structural properties of Al-5.6Zn-2.2Mg-1.3Cu composites using RSM: fabrication, characterization, and modelling,” *Heliyon*, vol. 8, 2022, Art. no. e10602. <https://doi.org/10.1016/j.heliyon.2022.e10602>.

Declaration of interests

The authors declare that they have no known competing financial interests or personal relationships that could have appeared to influence the work reported in this paper.

The authors declare the following financial interests/personal relationships which may be considered as potential competing interests:

Journal Pre-proof